Covalent Functionalization of Graphene Oxide-Characterization and Its Electrochemical Performance for Supercapacitor

Name: Safina Iram Javed
Reg No: NUST201260699MSCME67712F

This work is submitted as a MS thesis in partial fulfillment of the requirement for the degree of

(MS in Materials and Surface Engineering)

Supervisor: Prof. Dr. Zakir Hussain

School of Chemical and Materials Engineering (SCME)
National University of Sciences and Technology (NUST)
H-12, Islamabad, Pakistan

October, 2015

Certificate

This is to certify that the work in this thesis has been carried out by **Ms. Safina Iram Javed** and completed under my supervision in nano-materials laboratory, School of Chemical and Materials Engineering, National University of Sciences and Technology, H-12, Islamabad, Pakistan.

Supervisor _____

Prof. Dr. Zakir Hussain
Materials Engineering Department
National University of Sciences &
Technology, Islamabad

Submitted through

Prof. Dr. Mohammad Mujahid
Principal/Dean,
School of Chemical and Materials Engineering
National University of Sciences and Technology

ACKNOWLEDGEMENT

All praise to ***ALMIGHTY ALLAH,*** Who is the Lord of worlds. Whose presence has been figured on two words ***KUN-FAYA-KUN.*** Countless thanks to Him, Who bestowed upon me the potential and ability to contribute a drop of material in existing ocean of knowledge. All respects and regards to the ***Holy Prophet (PBUH)*** for enlightening our conscience and leading us on right path of believers, who is forever a source of inspiration and guidance for the mankind.

I feel great pleasure in expressing my deep gratitude to my respected teacher ***"Prof. Dr. Zakir Hussain"*** for his guidance, cooperation, valuable comments and intellectual suggestions, throughout the completion of this research work.

I feel obliged to pay my gratitude to all my respectful and honorable teachers, during my post-graduate studies, ***Dr. Muhammad Mujahid, Dr. Muhammad Shahid, Dr. Amir Habib, Dr. Nasir Mahmood, Dr. Muhammad Israr, Dr. Faheem Hashmi and Dr. I. H. Gull,*** who provided me with captivating experience and guidance at SCME.

I wish to thank my lab fellows, ***Farhana, Sumayya, Fakhar, Awais, Hina, Hareema, Zaib, Shehrish*** and PhD scholar ***Mr. Aftab Akram*** for their help and support during my research work.

I wish to thank my affectionate parents, ***"Mr. and Mrs. Javaid Amjad"*** for their never ending love and affection in all my efforts and for giving me the foundation to be who I am. I also thanked to my Sisters and Brothers for being so loving and compassionate. No words of acknowledgment can be adequate to the support and co-operation of my friends and colleagues, ***Amina, Tuba, Atia, Shazia, Mahpara, Sobia and Sikandar.***

Finally, I would like to pay special thanks to my husband ***Ahmad Muslim*** for his continuous support and encouragement during all the period. Without his encouragement and understanding it would not have been possible for me to complete this work. Thank you Ahmad, for taking good care of me.

Safina Iram Javed

DEDICATIONS

Each word of mine is dedicated to my Beloved Parents

Mr. JAVAID AMJAD and MRS MAQSOOD AKHTAR

Whose prayers and affection is the source of strength for me in every step of my life and a sign of success for my bright future.

To my lovely Brothers

TOSEEF JAVAID and NAFEES JAVAID

To my beloved sisters

TASLEEM JAVAID and NORINA IRAM

To my loving husband

AHMAD MUSLIM

Who are the blessings of Allah-Almighty,

Who are the sources of Inspiration,

Who are the dear most and

Who enabled me to accept all the challenges in my life

THANK YOU, I LOVE YOU All!

ABSTRACT

There has been a remarkable advancement in graphene research since the famous discovery in 2004. Research on graphene has revealed huge theoretical and practical advantages such as large surface area, excellent conductivity, very good capacitance and relatively low production cost. Graphene, simply a single layer of carbon atoms, is progressively making its room into a wide range of applications, from nano-composites to biosensors to supercapacitors to flexible/transparent displays. Graphene oxide (GO), a derivative of graphene has proved a feasible route to the accessibility of graphene through chemical ex-foliation process.

In the present work, graphene oxide was synthesized through chemical ex-foliation process from graphite flakes. GO was further covalently functionalized with Levofloxacin (LOF) by Steglich esterification reaction. Herein, we describe a method for the chemical functionalization and in-situ reduction of graphene oxide by LOF. GO was reduced and remained well dispersed after reduction in the solution even after 6 months. The functionalized and reduced GO was characterized through range of analytical techniques. Functionalized GO was further used as a supercapacitor (SC) electrode material and its electrochemical behavior was compared with GO and reported. Capacitance of functionalized GO was found to be four times the capacitance of GO, indicating significantly enhanced electrochemical performance of functionalized GO as compared to pure GO.

Table of Contents

List of Figures:

List of Tables:

List of Abbreviations:

GO	Graphene Oxide
rGO	Reduced graphene oxide
LOF	Levofloxacin((S)-9-fuoro-2,3-dihydro-3-methyl-10-(4-methyl-1-piperazinyl)-7-oxo-7H-pyrido[1,2,3-de]-1,4-benzoxazine-6-carboxylic acid)
DCC	*N,N′*-dicyclohexylcarbodiimide
DMAP	4-dimethyl-amino-pyridine
DMSO	Dimethyl sulfoxide
IPA	Isopropanol
Na_2SO_4	Sodium sulphate
RPM	Rotation per Minute
SEM	Scanning Electron Microscope
XRD	X-Ray Diffraction
FT-IR	Fourier Transform Infrared
UV-Vis	Ultraviolet-visible spectroscopy
CV	Cyclic Voltammetry
GO-Al	Graphene oxide coated on Aluminum foil
***f*-(LOF)GO**	Functionalized graphene oxide

Chapter 1

1 Introduction

1.1 Motivation

The alarming global energy crisis is demanding serious efforts to find renewable and durable energy sources that will finally substitute fossil fuels. Batteries being an energy source for many devices possess high energy density but they observe long charging cycles. Because of this limitation of batteries, electrochemical capacitors known as supercapacitors are used for power delivery and short recharging cycles. Regenerative braking, in hybrid cars and electric vehicles, is an application in which supercapacitors are used to recover power instead of dissipating brake energy as heat. On the other hand, supercapacitors possess low energy density. Despite the fact that different phenomena define the relative energy and power density of both supercapacitors and batteries still both rely on electrochemical processes.

Supercapacitors, as the energy storage devices, has been developed and industrialized nearly 40 years ago. Still there is requirement to improve its performance and to find new active electrode material due to the existing demands of energy storage in many applications like stop-start operation in hybrid vehicles**,** requirement of short term high power pulses in industrial backup systems. Electric double layer capacitors EDLCs, a class of supercapacitors, are capable of performing these tasks. They possess high power density, long cycle life than batteries and also possess high energy density as compared to traditional capacitors. When such kind of electrochemical capacitor is joined with a battery or fuel cell it is called hybrid energy storage device. Such capacitors usually use carbon as the active electrode material both for cathode and anode with aqueous / organic electrolytes.

During the last 6 to 8 years, there has been a remarkable expansion in research in the area of energy storage for exploring new materials that will possess high energy density, extended cycle life and short charging/discharging cycles.

The vision of developing materials having the energy density of battery, extended cycle life along with the power density of supercapacitor is an inspiring direction that so far has to be accomplished. Proper assessment of new energy materials as well as their charge storage means will assist development in the domain of electrochemical energy storage.

Chapter 2

2 Literature survey

2.1 Graphene and its applications

Graphene, a flat mono layer of carbon atoms which is packed into a honeycomb lattice (2D), is a basic element for all graphite materials.

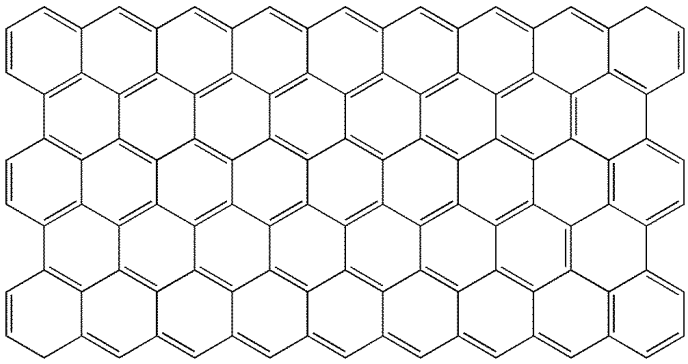

Figure 2.1 Structure of graphene

It can be transformed in the form of (0D) fullerenes, (1D) nanotubes or (3D) graphite as shown in figure 2.2(a) [1]. Figure 2.2(b) shows TEM image (bright field) of suspended single layer graphene sheet.

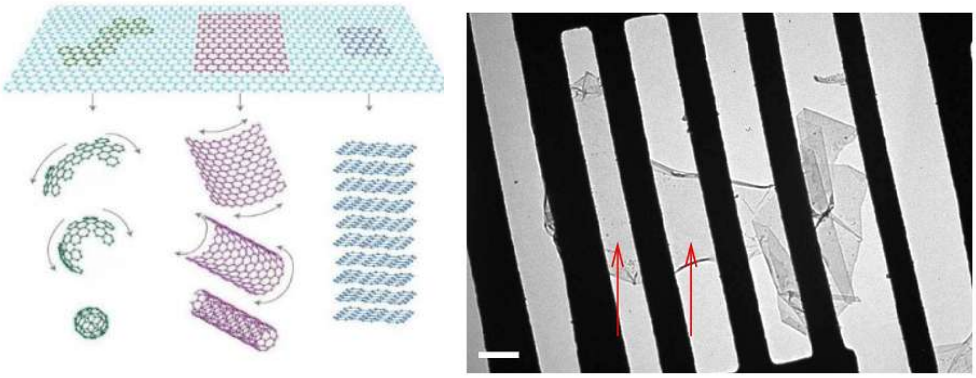

Figure 2.2 (a)Graphene a two dimensional building block for all carbon materials that can be wrapped up into buckyballs, rolled into nanotubes or stacked into graphite [1], (b)TEM image (bright field) of suspended graphene sheet. Arrows shows single layer graphene (scale bar 500 nm) [3].

Freely suspended graphene exhibit intrinsic ripples which appeared due to thermal fluctuations with a size distribution of 7 nm [2]. Freely suspended graphene sheets are stable due to the presence of these three dimensional elastic deformations[3].

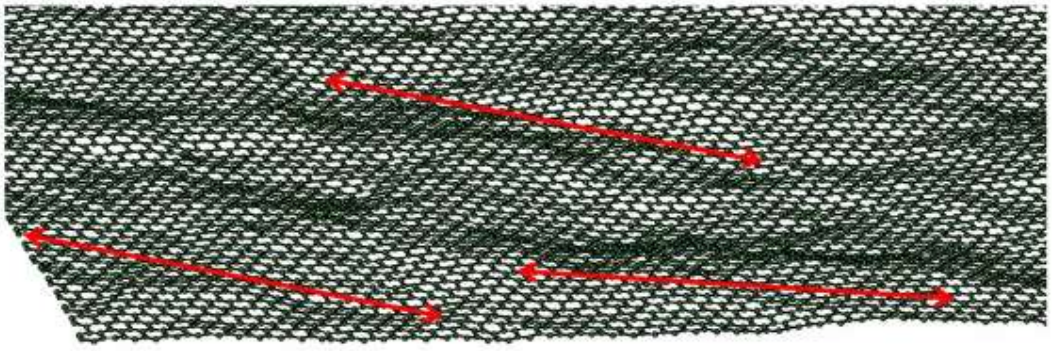

Figure 2.3 Graphene at room temperature based on Monte Carlo simulation (arrow length 7 nm) [2]

Research on graphene has revealed huge theoretical and applied advantages like large surface area, exceptional conductivity, very good capacitance, and relatively low fabrication cost [4]. Because of its tremendous mechanical [1], electrical [5], thermal [6], and transport characteristics [7] it has found many potential applications in sensors, nano-composites, supercapacitors and hydrogen storage.

2.2 Synthesis of Graphene

Various method have been exploited for the synthesis of graphene including both bottom up and top down approaches as described below.

- Bottom up

1. Chemical vapor deposition
2. Organic synthesis
3. Epitaxial growth

- Top down

1. Mechanical exfoliation
2. Wet chemical synthesis
3. Unzipping of CNT's

All the methods have their own advantages and disadvantages. Challenges are there for the production of large scale, high quality graphene in a cost-effective way. Graphene of highest quality can be produced by mechanically exfoliating crystalline graphite [8]. However, the amount of graphene produced by this method is small and is sufficient for research purposes only [3]. Current progress, particularly in the CVD growth of graphene using metal as substrates, exhibited excellent potential for its commercialization. Graphene synthesized by CVD usually display various domains, significantly limiting its performance due to decrease in its electrical conductivity. Further improvements like low growth temperature and easy transfer process for graphene synthesized by CVD, will permit advanced applications of graphene. Chemical oxidation of graphite into graphene oxide (GO) [9] then its subsequent reduction by hydrazine hydrate [10] is an alternate method that has been used widely for the mass production of graphene.

2.3 Graphene oxide (GO)

Graphene oxide can be fabricated by the Brodie [11], Hummers [12], Staudenmaier [13] and improved hummers methods [14]. A typical synthesis starts with the oxidization of pristine graphite, during which various chemical groups are adhered to the surface of carbon planes. These intercalated chemical groups weaken the Van-der-Waals forces present between carbon planes.

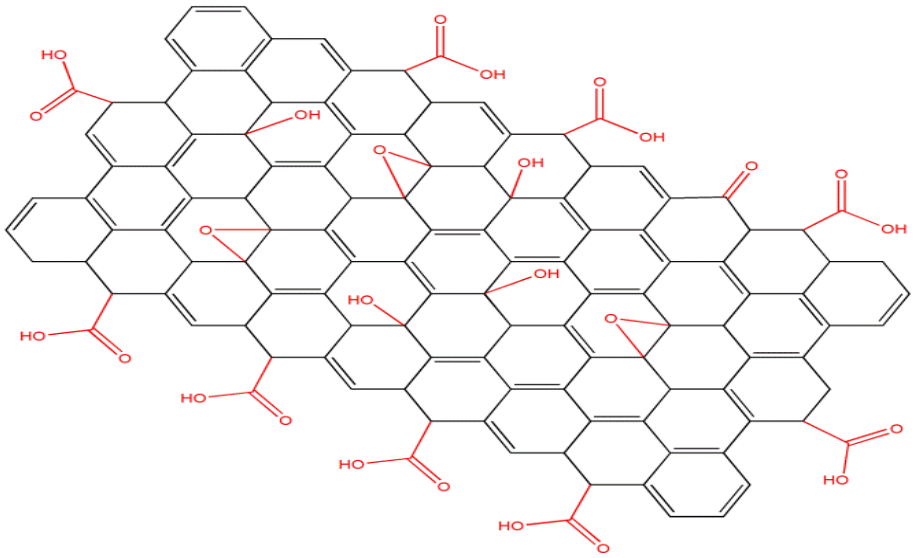

Figure 2.4 Schematic of GO

The two terms graphite oxide and graphene oxide are different from each other. Exact chemical structure of graphite oxide has still been considered for debate and no explicit model has been finalized yet [15]. During the oxidation of graphite, interplanar distance between the graphene sheets increases, and van der Waals forces decreases. Hence, graphite oxide is graphite where oxygen containing functional groups are incorporated between the graphitic layers. Chemically, GO is very similar to graphite oxide, but in terms of structure both are different. Instead of keeping a layered structure, it is exfoliated into single/a few stacked layers, and a number of reactive oxygen functionalities are present on graphene oxide [15].

There are two kinds of regions present in the structure of GO: a region containing unoxidized carbon atoms called aromatic region and the regions having carbon atoms bonded to different chemical groups. The degree of oxidation defines the relative dimension of oxidized and aromatic regions. A considerable fraction of the oxidized region contains carbon atoms bonded to epoxy or hydroxyl groups whereas small fractions are bonded to carbonyl, ketone or carboxylic groups at the carbon plane edges. These functional groups are present on both sides of the graphitic plane [16, 17]. Hydrophilic nature of GO is attributed to the existence of these functionalities attached to the carbon plane, hence GO forms very stable aqueous dispersions.

Prepared graphite oxide, is then separated into graphene layers with the help of thermal treatment or graphite oxide can be used to produce aqueous dispersion of graphene oxide (GO) sheets via ultrasonication procedure. The electrostatic repulsion forces between graphene oxide layers are responsible for the stabilization of these suspensions [18]. The procedure is shown in Figure 2.5

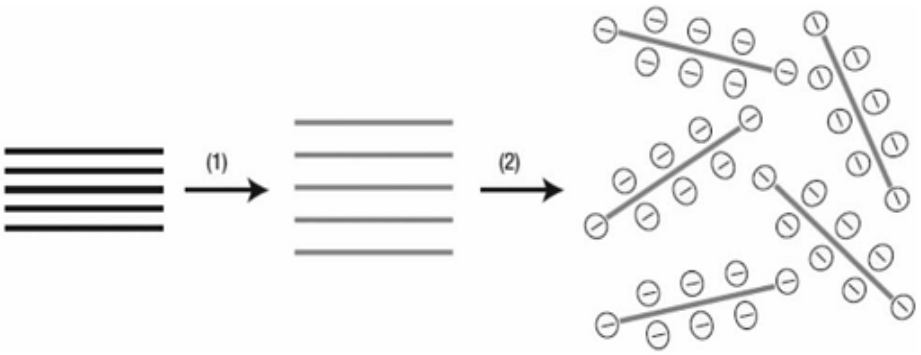

Figure 2.5 Schematic for the synthesis of GO dispersions through chemical route (1) Increase in interlayer spacing of graphitic planes during the oxidation leads to the formation of graphite oxide (2) sonication plus exfoliation of graphite oxide and stabilization of GO suspension via electrostatic repulsion [18]

Hydrophilic character of GO is due to the attachment of oxygen functional groups. As a result, water molecules intercalate between consecutive carbon planes. So GO can be considered as a graphite based intercalation compound containing covalently bonded oxygen and non-covalently bonded water molecules between graphitic layers [19]. Figure 2.6 shows the hydrogen bonding between oxygen functionalities of GO and water.

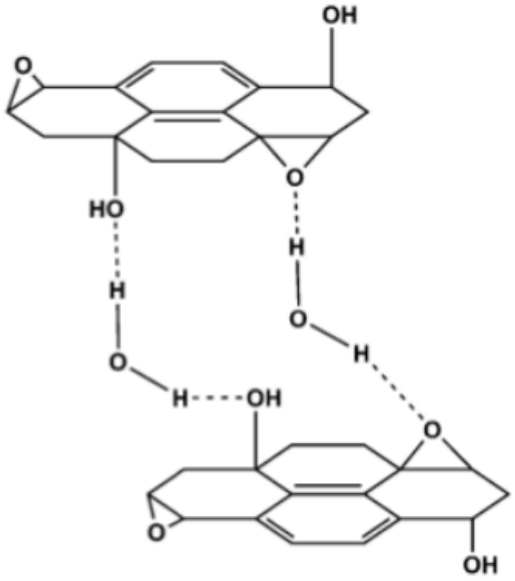

Figure 2.6 Representation of hydrogen bonding between functional groups of GO and water [15]

Chemical reduction of GO [20] or thermal annealing [21] are two methods used for the restoration of intrinsic properties of graphene [22, 23]. After chemical intercalation in the oxidation process of graphite, GO can be separated into single graphene sheets by thermal exfoliation. During which both processes, exfoliation of graphene sheets and elimination of the attached oxygenated groups, occur altogether. During a rapid heating decomposition process, the hydroxyl and epoxide groups decomposes into H_2O, CO_2 and CO that builds up high enough pressures to surpass the Van der Waals attractive forces binding the graphene sheets [24]. Thermal expansion must be carried out at a high rate to produce large pressure that overcomes the Van der Waals forces [21, 24]. Graphite oxide was expanded into graphene by thermal shock and the product obtained after the thermal annealing was further treated with ultrasonic irradiation as reported by Chen et al. [25].

In addition to the heat treatment of GO in an ultrahigh vacuum, the procedure can be performed in different atmospheres like argon and hydrogen. GO can be prevented from contamination during the reduction process if thermal treatment is carried out in an Argon atmosphere. The reduction of graphene oxide was enhanced when the process carried out in the presence of hydrogen, as indicated by higher C/O ratio [26]. Simulations depict that the presence of hydrogen can improve the reduction efficiency by 3.3% to 7.4%. This is because of the transformation of epoxies and carbonyls into hydroxyl which decomposes into water upon heating [18]. Thermal exfoliation of GO can be used to prepare graphene sheets of high quality by controlling the gas atmosphere, duration and heating temperature. Whereas the elimination of oxygen functionalities leads to a mass loss up to 30% creating vacancies and defects in the carbon planes which extensively influence the electrical and mechanical properties of graphene sheets.

Chemical reduction of GO is another commonly used method for the restoration of the properties of graphene as these techniques are simple and availability of reducing agents at low price. Hydrazine (N_2H_4), Aluminum/Iron powder, alcohol, Sodium/Potassium hydroxide, ascorbic acid and Sodium borohydride ($NaBH_4$) are used for the reduction of GO [18]. Hydrazine is the most commonly used reducing agent due to the fact that it produces high quality graphene at low temperature and its zero reactivity towards water. Stankovich et al. firstly proposed the reduction mechanism of graphene oxide by hydrazine as shown in Figure 2.7 [19].

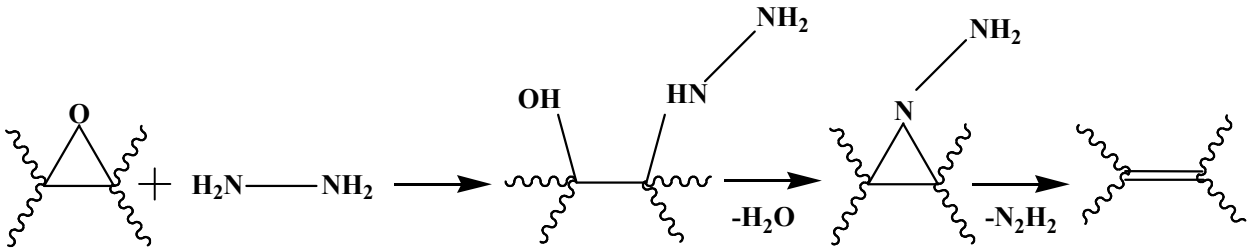

Figure 2.7 Reduction mechanism of GO by hydrazine [19]

Figure shows that the epoxy ring is opened by the extraction of hydrogen from hydrazine, transforming into hydrazine alcohol. Then hydrazine alcohol molecule transports one hydrogen atom to the hydroxyl group and discharges one water molecule. The resultant product then experiences thermal removal of di-imide creating a double bond. In this way conjugated network is re-established in graphene sheets.

Hydroxyl and epoxy groups are mainly eliminated by this method but other groups like carbonyl and ketone, present at the edges are still attached. Besides XPS results indicate that during the reduction process side reaction may occur resulting in the formation of C-N groups at the rGO surface hence presenting low electrical conductivity nearly 2000 S/m [19]. C-N groups and other functional groups are eliminated by performing post-thermal annealing that results in high electrical conductivity from 11,800 to 35,100 S/m [27]. $NaBH_4$, another widely used reducing agent, generally eliminates epoxy groups but cannot remove hydroxyl or carboxyl groups. Hence low electrical conductivity up to 45 S/m is presented by rGO sheets produced in this method [28].

Since $NaBH_4$ and hydrazine based[29] chemicals are toxic, environment friendly reducing agents have been explored for the preparation of good quality graphene.

2.4 Functionalization of GO

Functionalization can be accomplished in two ways. Either to covalently attach external atoms directly with the carbon of graphene that leads to the tuning of electronic structure and formation of defect sites or to covalently couple the native functional group of GO with the guest functional group. The structural modification may occur on the carbon plane and/or at the sheets edges. Along with diverse electrical properties compared to undoped graphene, increased thermal stability and mechanical strength is also achieved as a result of functionalization [30].

2.4.1 Covalent functionalization

During the covalent functionalization the structural modification may occur on the carbon plane and/or at the sheets edges. The covalent functionalization of graphene can be realized by four different approaches such as:

- Nucleophilic substitution
- Electrophilic addition
- Condensation
- Addition reaction

In nucleophilic substitution, the epoxy functionalities of graphene oxide behave as the active spots. Amine functionalities, present in the organic compound to be coupled with graphene, bear electron lone pairs and attacks the epoxy sites on the basal plane of graphene oxide. Nucleophilic substitution is comparatively an easy process that can be executed both at room temperature and in aqueous solutions. Hence it is mainly used for mass production of covalently coupled graphene. Functionalization of graphene has been achieved by various kinds of aromatic and aliphatic amines, ionic liquids, amino acids, silane compounds and small molecular weight polymers[31-34].

In the electrophilic substitution reaction, a hydrogen atom of graphene is displaced by an electrphile. As an example, attachment of the diazonium salt (of para-nitro aniline) to graphene is accomplished by the electrophilic replacement [35].

In a condensation reaction, two functional groups combine and one single molecule is formed along with the entropy loss. Condensation on the graphene takes place through the development

of amides and carbamate ester links [36]. surface modification of GO using various isocyanate compounds was carried out by Stankovich et al. [37, 38].

In addition reactions, two or more molecules are combined and transformed into a larger molecule [36]. Using the same perception, a cyclo-addition reaction was used to functionalize graphene with azidotrimethylsilane [39].

This approach can be used to covalently attach various kind of polymers and functional moieties

This approach allows various functional entities and polymers to covalently adhere to the graphene. Functionalized graphene obtained by this method exhibits electrical conductivity ~ 0.1-1000 S $m^{-1}$and shows good dispersibility in water, toluene, chloroform and DMF [36].

2.4.2 Non-covalent functionalization

This type of functionalization is mainly carried out with the help of Van der Waals, hydrophobic and electrostatic interactions. As a consequence organic molecules get physically adsorbed on the graphene surface. Non-covalent functionalization is realized by adsorption of small aromatic molecules or surfactants, polymer wrapping. It is a distinguished protocol used for the surface modification of graphitic materials [36].

2.5 Graphene an emerging material for Supercapacitor applications

2.5.1 Evolution of capacitor to supercapacitor

Capacitors, a basic electric circuit element, is used for the storage of electrical energy in microfarads and also used as a filtering element There are two main functions of capacitors

1. Use to charge/discharge electricity in smoothing, backup and timer circuits of different electrical appliances

2. To block direct current in filter circuits for the elimination of particular frequencies

1st generation capacitors are electrostatic capacitors. Electrolytic capacitors, next generation capacitors, are analogous to batteries with respect to the cell structure. Unlike batteries, in capacitors cathode and anode are made of the same materials. Solid/liquid electrolytes have been used in tantalum, aluminum and ceramic capacitors [40].

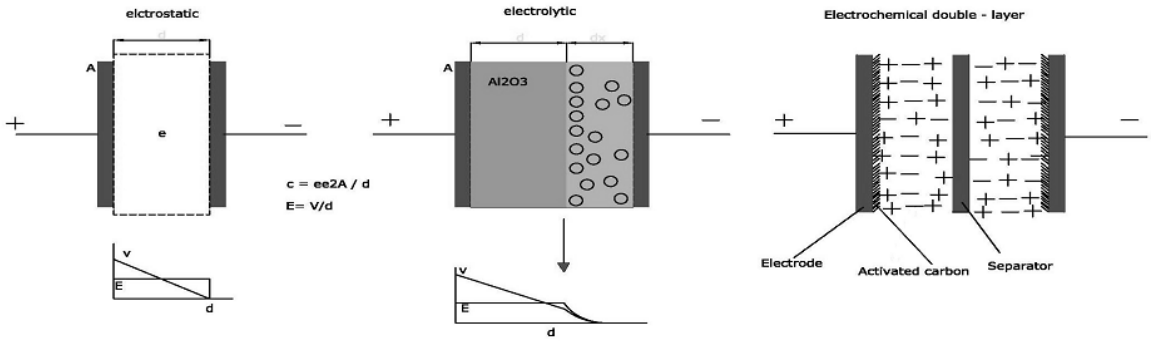

Figure 2.8 Schematic diagram representing electrostatic, electrolytic and electrical double layer capacitor [40]

The third generation of capacitors is supercapacitor, in which the electric charge accumulated at the electrolyte/metal interface caused by the electrostatic attraction, is used to create a storage mechanism. Electrical charge of the order of ~10^6 Farad can be stored at this interface [40]. Activated carbon is the main component used for the electrode construction in EDLC. Electrode surface area, the electrochemically active area is the main factor determining the capacity of supercapacitor. This electrochemically active area is different from physical surface area determined by nitrogen physisorption [41].

Two main mechanisms further classify supercapacitor into

(1) Electric double layer capacitor (EDLC)
(2) Pseudocapacitor

Charge is stored electrostatically in EDLC during reversible cycles of adsorption–desorption of electrolyte ions on the electrode surface. Following are the properties of EDLC electrode material

- Large accessible area
- Electrochemically stable
- Not favorable for Faradic reaction

Since charge storage occurs at the electrolyte/electrode interface, it allows quite fast energy uptake/delivery hence superior power performance. But at the same time polarization of the electrode and physicochemical process limits its energy density.

Alternatively, reversible Faradic reaction occurs on the electrode surface in pseudocapacitor. Different types of electrode materials have been used in pseudocapacitor e.g. metal oxides [42], chemically modified carbon materials [43, 44] and conducting polymers [45, 46]. Though pseudocapacitor possesses relatively high energy density with respect to EDLCs, their cycling stability is poor. Also they show longer response time since longer times are required for electron movements in redox reactions accruing at the electrode surface [47].

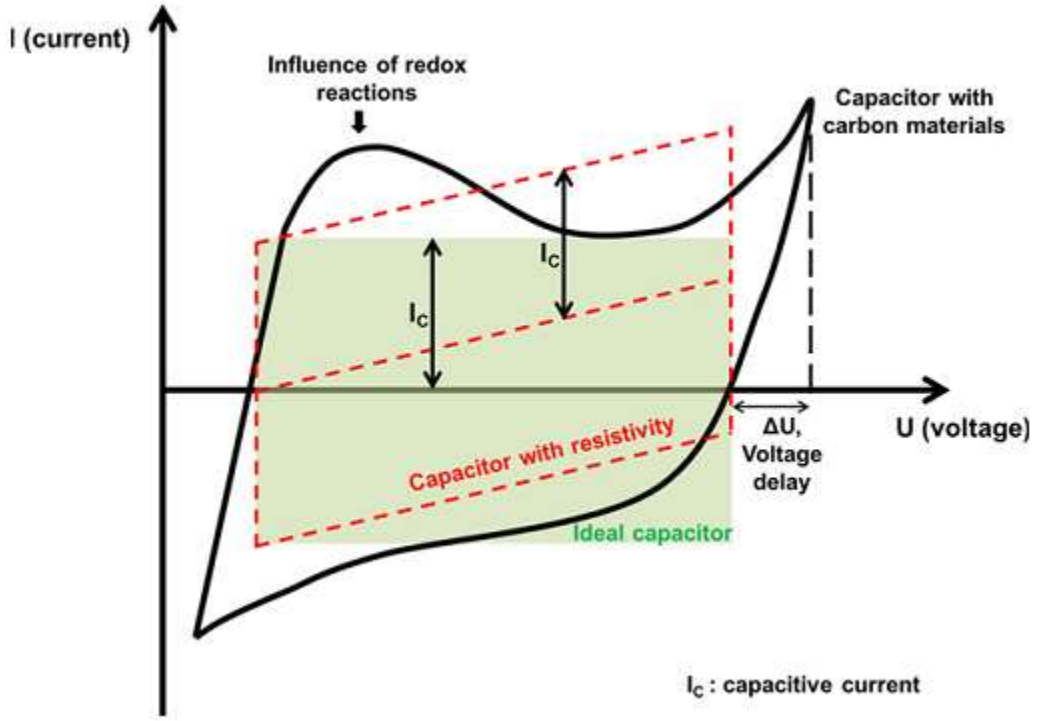

Figure 2.9 Schematic representation of voltammetry response curve of supercapacitor [47]

Key factors [48] controlling the performance of a supercapacitor are

- Electrolyte
- Separator thickness
- Electrode properties (porosity, mechanical stability, volume, resistance)

Graphene has been emerged as a promising material for supercapacitor applications, due to its outstanding properties over the conventional carbonaceous materials. As an electrode material for supercapacitor: graphene possess large surface area (2630 m^2/g) [49], very good thermal [50] and electrical conductivity (4840– 5300 W/m K, $2x10^2$ S/m) [49] as well as theoretical double layer capacitance (~21 $\mu F/cm^2$) [51].

Graphene due to its intrinsic large surface area offer electro-active sites, facile accessibility to electrolytic ions and promising electrical conductivity which in turn facilitate transportation of electrons mainly for pseudocapacitor.

Despite of the small energy density (nearly5–10 W h/kg) of Electrochemical capacitors (EC), they charge and discharge in seconds maintaining high power density (10 kW/kg) [52].

Therefore, EC possess high power capability and fast charge/discharge rate and are safer than batteries in terms of short circuiting by self-ignition. They also possess durability for long cycles and do not contain toxic materials [48].

Chapter 3

3 Synthesis and Characterization Techniques

3.1 Synthesis technique for GO

Graphene oxide (GO) can be produced by means of a simplified Hummer's method in which oxidation process is executed at room-temperature. This method has been reported for the synthesis of high-yield and large-area Graphene oxide [9]. Basically the synthesis protocol can be divided into seven basic steps, as described below.

Step 1 – graphite powder + H_2SO_4 +H_3PO_4+ $KMnO_4$

Graphite powder (1 g), H_2SO_4 and H_3PO_4 in 9:1 ratio (120:13) ml and $KMnO_4$ (3 g) was mixed and magnetically stirred at 25 ^oC for 3 days. This acidic blend oxidized the graphite flakes in the presence of $KMnO_4$ [9].

Step 2 – the addition of H_2O_2

Upon the addition of hydrogen peroxide to the oxidized mixture, the remaining permanganate and manganese dioxide reduced to soluble colorless manganese sulfate, and the dark brown color of the mixture was turned to yellow [12].

Step 3 – washing with 1:10 HCl

When the above mixture was rinsed with a solution of 1:10 HCl, the metal ions were removed from the product [53].

Step 4 – washing with water until the pH is 7

Washing was performed to increase the pH of the oxidized graphite mixture. Hydrophilicity of the graphene oxide is largely affected by the pH and the desired properties can be achieved at the pH of 7. Carboxyl groups, present on the graphene oxide surface, are protonated at low pH and as a result of that graphene sheets turn out to be less hydrophilic and aggregate with each other. At high pH the de-protonated carboxyl groups become so hydrophilic that individual sheets have a preference to dissolve in water resembling common salts [54].

Step 5 – ultrasonication for making aqueous dispersion

Ultrasonication was used to disperse the graphite oxide paste into water and as a result it was exfoliated and turned into graphene oxide [53].

Step 6 – centrifugation

After making the aqueous dispersion of GO by ultrasonication, it was centrifuged to remove any un-exfoliated graphite oxide and supernatant was separated [55].

Step 7 – vacuum drying the graphene oxide at low temperature

This step performed to remove the excess water and since drying was carried out in vacuum at low temperature (~ 40 ^{o}C), sheets of graphene oxide were obtained without any change in chemical structure.

3.2 Functionalization of GO

With hydroxyl groups present on the basal plane of GO and carboxyl functional groups on the structure of LOF, Steglich esterification reaction catalyzed by DMAP and DCC was employed for the synthesis of covalently functionalized GO. Esterification reaction represents a chemical reaction in which two participants react to form an ester. An esterification reaction is shown in figure 3.1

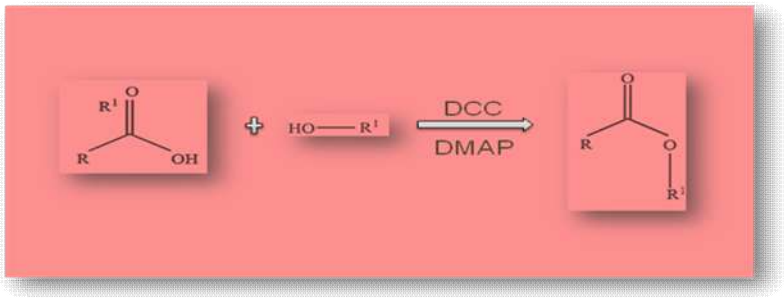

Figure 3.1 An esterification reaction

The un-reacted LOF was removed by centrifugation procedure, and various analytical techniques were employed to characterize the materials.

3.3 Fabrication of electrochemical test cell

After the successful functionalization of GO, the resultant product was characterized for its electrochemical performance keeping pristine GO as a reference material in our case. Simple drop cast and drying method was employed for the fabrication of supercapacitor electrodes [56]. Laboratory scale supercapacitor was tested by Cyclic Voltammetry in a two electrode configuration.

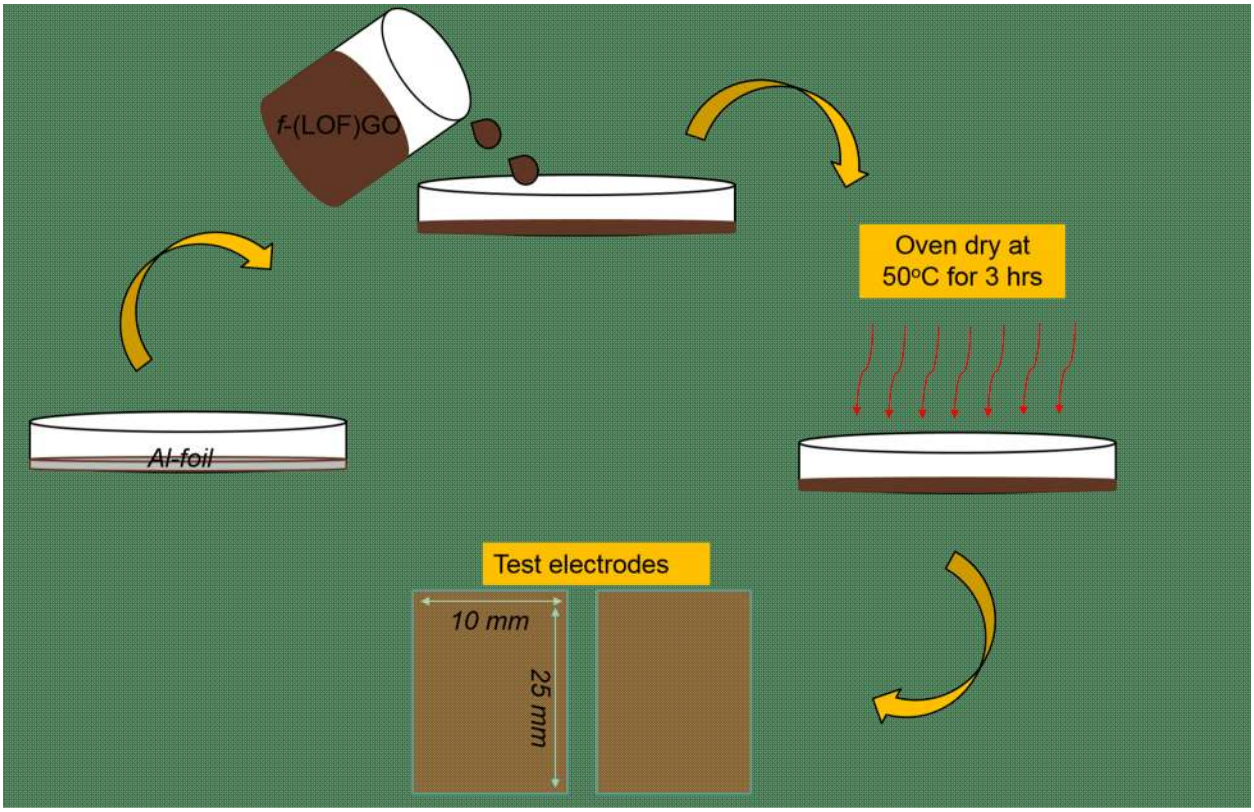

Figure 3.2 Illustration of supercapacitor electrode fabrication

3.4 Nano-material Characterization Methods

Different techniques have been used for the characterization of nano-materials. For nano-material characterization Particle-wave duality, such as photons and electrons, has been used to make direct or indirect interpretations. Electron microscopes use beams of electrons to explore materials microstructures while XPS and XRD are used to characterize atomic and lattice material with the help of X-ray photons. These techniques help to discover fine structural information accurately up to the nanometer scale since these beams possess short wavelengths and superior resolution in contrast to the visible light. These techniques have been described below:

3.4.1 X-Ray Diffraction (XRD)

Diffraction is due to the interaction between two or more waves that have the same frequency and a definite relationship in phase angles. XRD is used to evaluate the crystal structure of materials and its lattice characterization.

X-rays, a part of electromagnetic radiation spectrum, possesses short wavelengths hence large energies. These wavelengths are equivalent to the atomic spacing of solids. When x-rays are imposed on a solid, a part of the x-rays beam scatters at different angles by the ions that lie within the beam's path or by the electrons associated with each atom. In XRD diffractometer, a monochromatic and coherent x-ray beam (wavelength λ) is sent at an angle θ towards the specimen. As shown in figure 3.3, two parallel planes of atoms (A-A' and B-B'), with the same Miller indices (hkl) are separated by the interplanar spacing d_{hkl} [57].

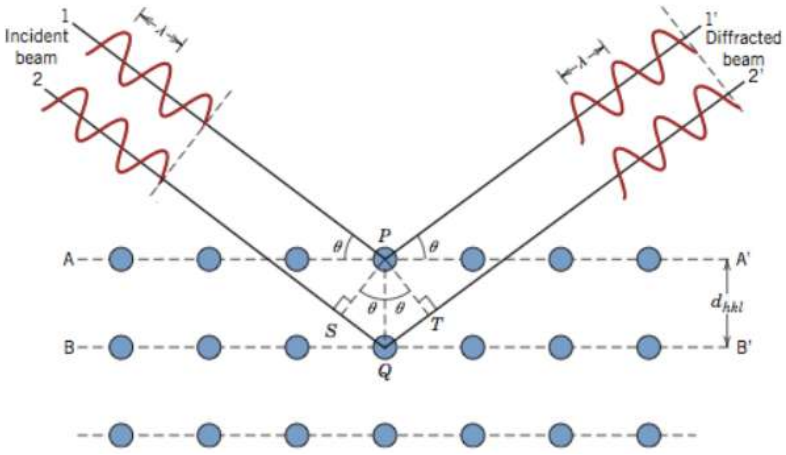

Figure 3.3 Diffraction of X-rays from atomic planes [57]

The phase relationship between the diffracted and the incident beam depends upon the path difference of the two beams. When their path difference is the integer multiple of wavelength, the diffracted beams will be in phase and will interfere constructively. But when the path difference is integral multiple of half wavelengths, diffracted beams will be out of phase and they will interfere destructively. So, the diffraction will occur when the following condition is fulfilled.

$$\boldsymbol{n\lambda = SQ + QT}$$

$$\boldsymbol{n\lambda = d_{hkl} \sin\theta + d_{hkl} \sin\theta}$$

$$\boldsymbol{n\lambda = 2d_{hkl} \sin\theta}$$

An X-ray diffractometer is presented in figure 3.4(b) used for the determination of the angles at which diffraction occurs. The specimen "S" is supported on a plate form in such a way that rotation about the axis ("O" perpendicular to the plane of paper) is possible. A monochromatic beam of X-ray is created from the target T, and diffracted beams intensities are detected with a counter, C. This counter is supported on a moving stage and its position (2θ) is indicated on a marked scale. The stage and sample are mechanically coupled so that a rotation "θ" of the sample is complemented by "2θ" rotation of the counter. Because of the coupling both angles (made by incident and reflected beams) remains same. When the diffraction pattern is obtained after certain amount of exposure to the radiation, it displays the intensities along y-axis, and the diffraction angle (2θ) along x-axis. The intensities in the diffraction pattern give information about the atomic arrangements within the lattice unit cell. The angular location of the diffraction peaks gives information about the unit cell size and its geometry. A unique powder x-ray diffraction pattern is associated with every crystalline material. The easiest way to recognize a compound is by making a comparing between the obtained diffraction patterns with the database containing diffraction patterns of known materials.

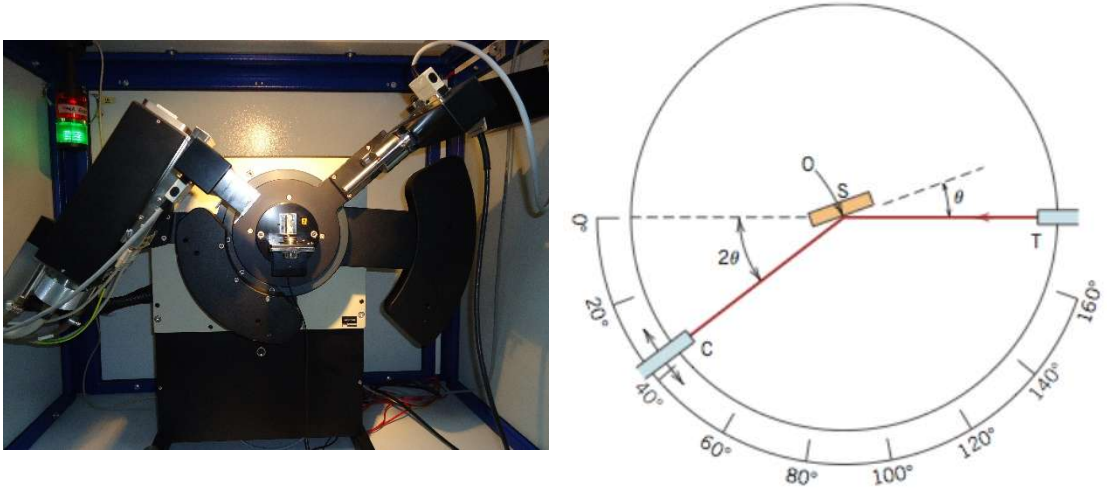

Figure 3.4 (a)The XRD system (STOE θ-θ), (b) Schematic illustration of an X-ray diffractometer [57]

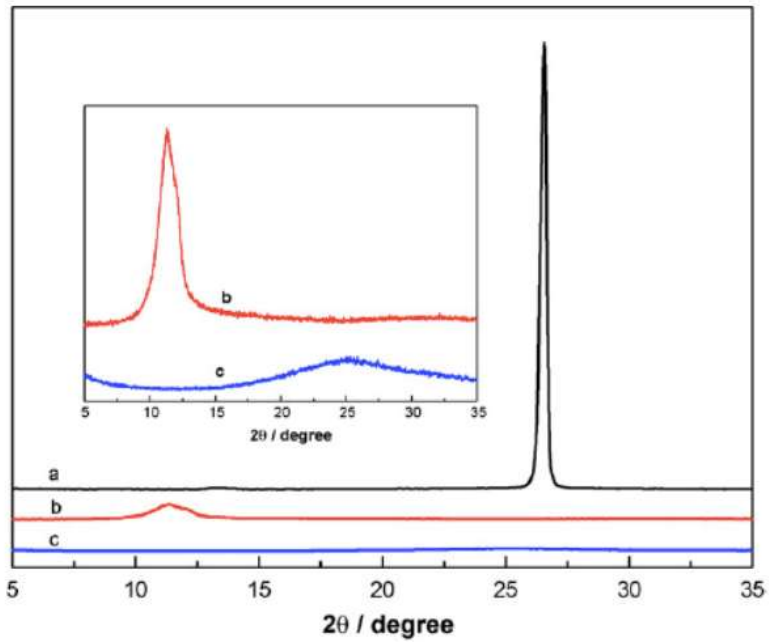

Figure 3.5 XRD patterns for graphite, GO and graphene [58]

Figure 3.5 shows the XRD graphs for graphene, GO and graphite. Diffracted peak (002) for graphite powder appears at 26.58° while in the case of GO, this peak disappears and a new diffraction peak can be detected at 11.36° whereas no diffraction peak is observed for graphene [58].

When considering XRD patterns there is another important equation called the "Scherrer's equation" [59],is given as

$$t = \frac{0.9\lambda}{B_{1/2} \quad cos\theta_B}$$

Where

t = crystallite size

λ= X-ray wavelength

θ_B= Bragg's angle

$B_{1/2}$ = Intensity at full width half maximum

So crystallite size (t) being an important parameter can be calculated from this equation.

In our case, the structural analysis of our samples was performed on XRD diffractometer STOE (θ- θ).

Above description has been established from the book "Materials Science and Engineering: An Introduction" of Callister and Rethwisch [57].

3.4.2 Optical microscopy

A compound optical microscope is also known as 'light microscope'. Visible light is used to create an enlarged image of the sample, such that it is reflected from the sample on the observer's eye through objective lenses (Or on the surface of a photosensitive imaging device). The word *compound* is used because these two lenses (objective and eyepiece), work collectively to generate the final magnification "*M"* of the image such as:

$$\boldsymbol{M_{final} = M_{obj} \times M_{oc.}}$$

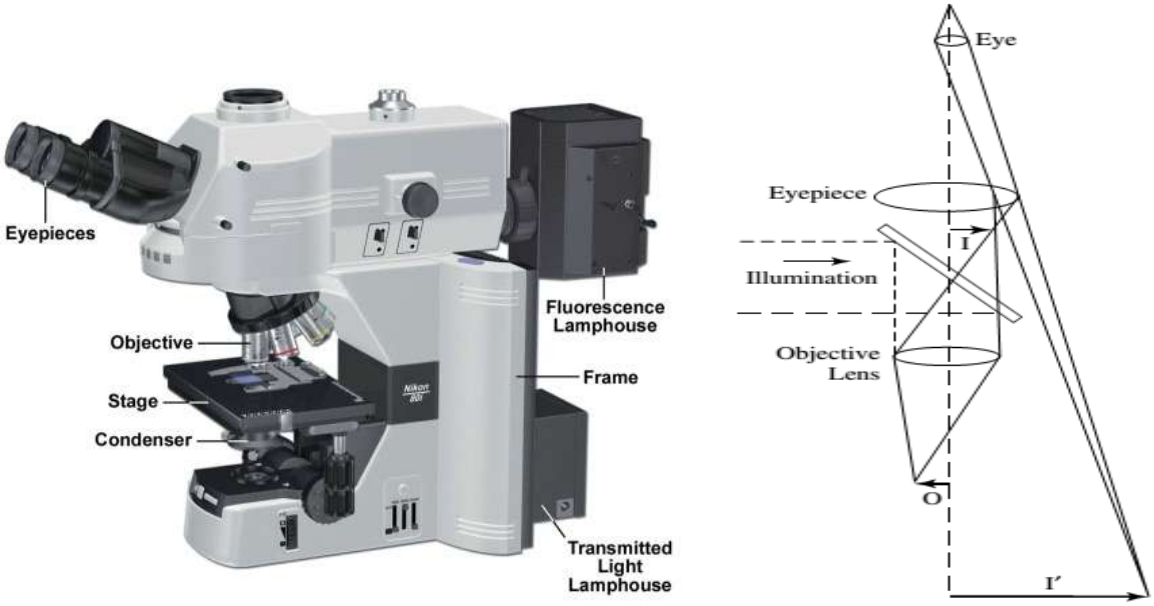

Figure 3.6 Compound microscope and schematic diagram of compound microscope's optical path [60]

Contrast of a microscope is the ability to distinguish different parts of an entity that depends on several factors. Image quality is degraded by dirty eyepieces/objectives. Glare is another factor that will diminish contrast, especially for highly reflecting samples. It becomes most severe when samples are being viewed with little contrast but it can be controlled to some level by controlling the aperture that controls the area of the illuminated region. This diaphragm should not be opened more than just sufficient to light up the field of microscope [60].

3.4.3 Scanning Electron Microscope (SEM)

The upper limit of the possible magnification with an optical microscope is approximately 2000X. For much higher magnifications and fine resolutions this limitation has defeated by SEM.

In this microscope, surface of the sample is examined by charged electronic beam [61]. A thermo-ionic gun (cathode) is used to discharge accelerated electrons by a voltage of 15 KeV.

The resultant incident electron beam is focused onto the surface of the specimen in a 10–100 nm spot by using magnetic condenser and objective lenses.

It produces images by examining the specimen surface with a focused electron beam. The sample surface is scanned in a rectangular pattern by the electronic beam. Secondary electrons are formed by the electronic interactions with the surface atoms of the sample, which are then detected with specialized lateral detectors and with zero magnetic fields at the specimen surface. After signal amplification, a magnified image (black and white) of the sample is presented with nanometer resolutions. Different grey scaled SEM images are formed owing to the diversity in the number of reflected electrons and also due to the difference in the energy of the reflected electrons. Elements with higher atomic number appear comparatively brighter than elements with lower atomic number.In this project, SEM analysis is performed by FEI scanning electron microscope (Nova NanoSEM).

The surface of the sample used for the analysis has to be electrically conductive. If the sample is non-conductive, a very thin metallic coating is applied on the surface of nonconductive materials. SEM images of the morphology of graphite GO and reduced graphene oxide are presented in figure 3.8 a, b and c respectively.

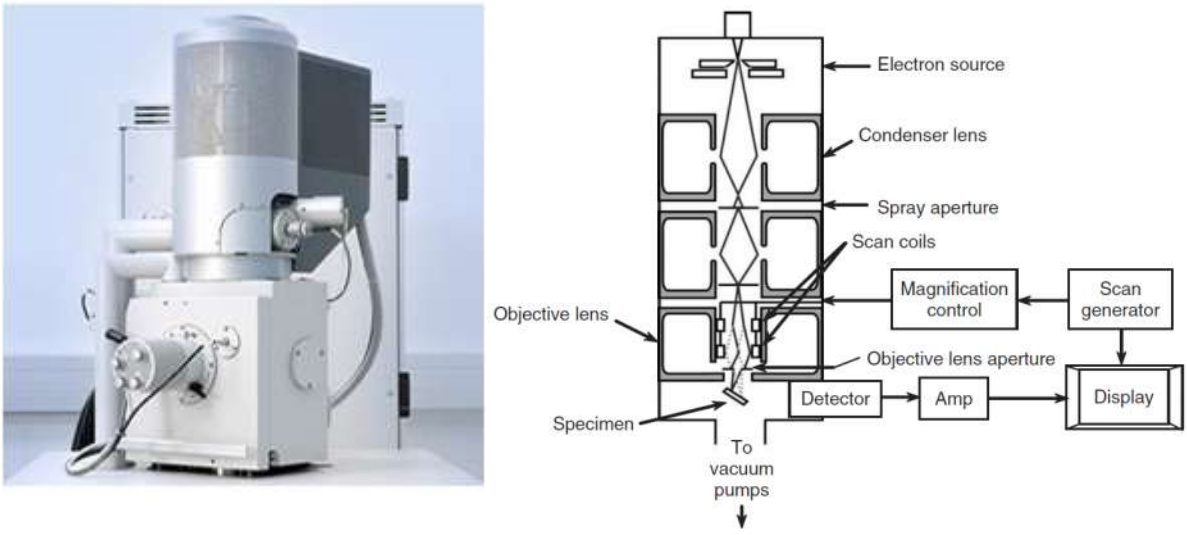

Figure 3.7 (a) The FEI Nova NanoSEM and (b) schematic of a SEM Adapted from Goldstein et al. (2003)

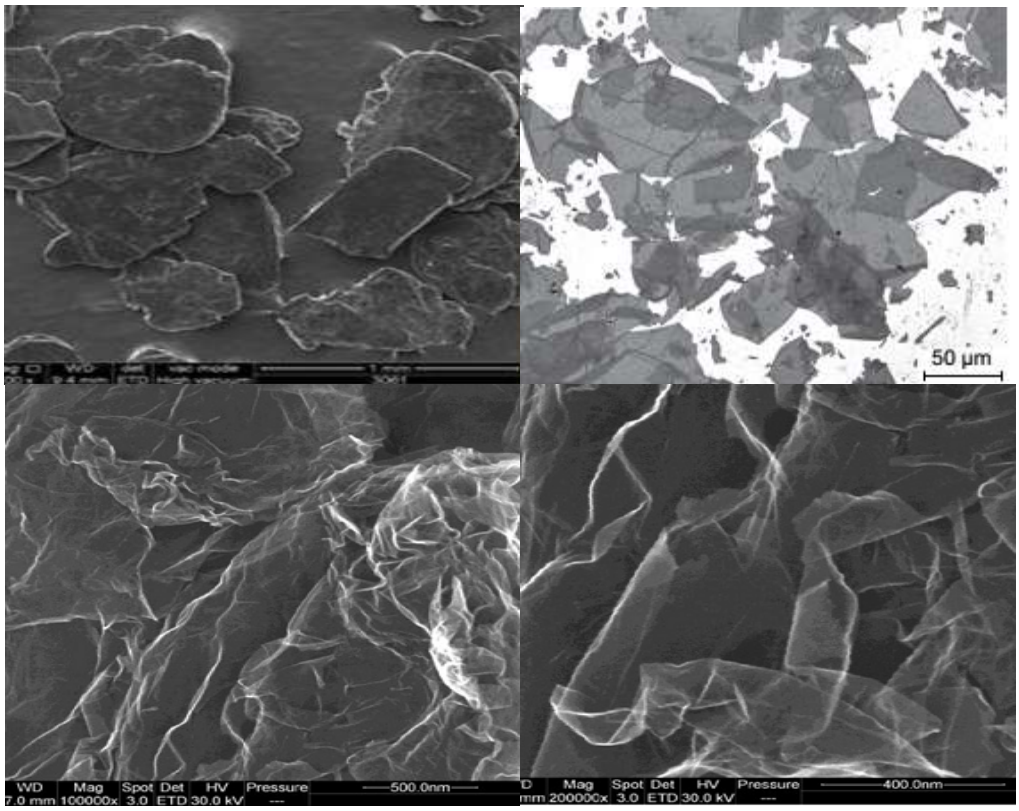

Figure 3.8 SEM image of (a) graphite [56], (b) GO [9], (c) graphene sheets [58]

3.4.4 UV-Vis Spectroscopy

UV-Vis spectroscopy is one of the old methods in molecular spectroscopy. UV-Vis spectroscopy along with additional physical techniques (like TEM, SEM, etc.) could be used to characterize nano-materials. Primarily, it could play an important role in verifying recommended mechanism for fusion or encapsulation [62]. Bohr-Einstein frequency relationship is the basis of Optical Spectroscopy as described below:

$$\Delta E = E2 - E1 = h\upsilon$$

Energy level range in the ultraviolet (UV) and visible (VIS) region for absorption spectroscopy can be characterized by the information [63] in Fig. 3.9

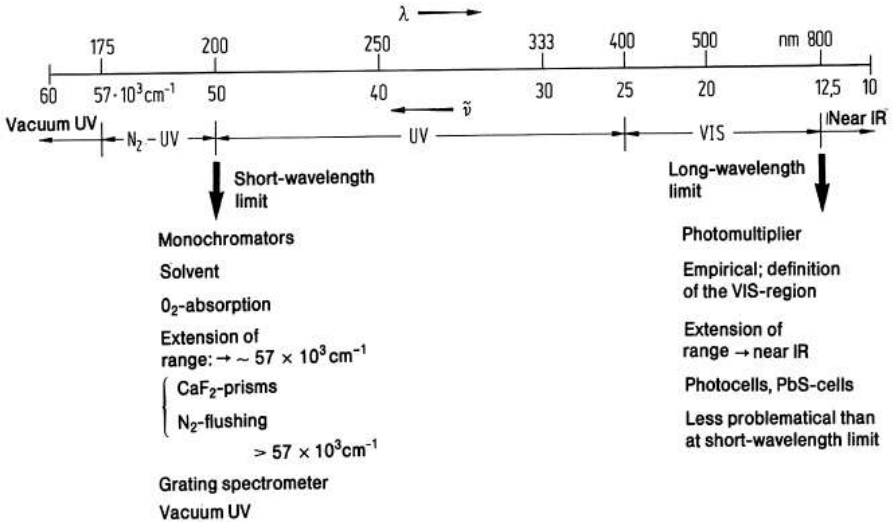

Figure 3.9 The electromagnetic spectrum representing UV, visible and IR wavelengths [63]

The basis for the identification and structural determination of UV-VIS spectroscopy is on the electronic ground and excited states of molecules depending upon the number of electrons, the structure, geometry and also the symmetry.

It is primarily employed to assess transmission and absorptions in fluids and solid materials. An array of light with wavelength (1100-200 nm) is impinged upon the sample and the reflected array is examined by the detector. When the light passes through the sample, different elements in the sample depending upon the nature of chemical bonds and structure will absorb light at various wavelengths. As a result electrons absorb photons and jump to an excited state (valence to the conduction band). A spectrophotometer records the wavelength at which absorption occurs and the information is displayed in the form of graph between the absorbance and wavelength.

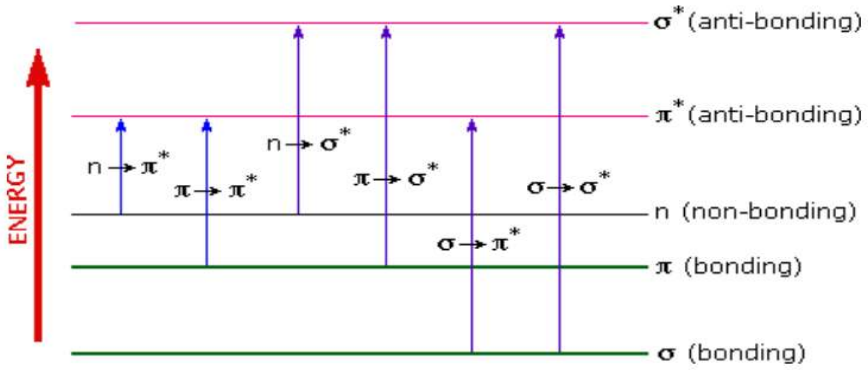

Figure 3.10 Representation of the Electronic transitions in materials

3.4.5 FTIR Spectroscopy

IR defines the interaction of infrared light and matter. FTIR is a special type of IR spectrometer which requires absorption spectrum in the infrared region[64].

The absorbance of radiation through the sample s is computed by using the given equation:

$A = \log (I_0/I)$

Whereas

A = Absorbance

I_0 = Intensity of the background spectrum

I = Intensity of the sample spectrum

After the absorption of infrared radiation, molecules get excited and jump to higher energy states. This absorption of IR radiation is similar to other absorption processes. It is a quantized process in which a molecule only absorbs preferred frequencies of IR spectrum. Energy absorbed during this process causes an increase in the amplitude of the vibration of the bonds of the molecule. Whereas, only those bonds with a dipole moment that changes with time can absorb IR radiation. Every type of bond possess an intrinsic frequency of vibration, two same type of bonds in two different compounds withstand different environments, hence no two molecules which own different structures have exactly the same IR absorption pattern [65].

It used to resolve the unknown concentration of the given samples by using the spectrum of samples of known concentration to set up a calibration line; linking absorbance to the concentration according to Beer's Law [66].

A = εlc

Whereas

A = Absorbance

ε = Absorptivity

l = Path-length

c = Concentration

This technique is mostly practiced in the semiconductor industry to verify the presence of dopant/impurity atoms. In this work, FTIR is used to determine different functional groups attached and present in GO, and disappearance of some of them in the functionalized GO. Figure 3.11 represents the schematic diagram of an FTIR spectrometer [67]. Measured transmittance will be plotted against the wavelength in FTIR spectrum. Figure 3.12 shows the regions where different types of bond absorb IR energies [68].

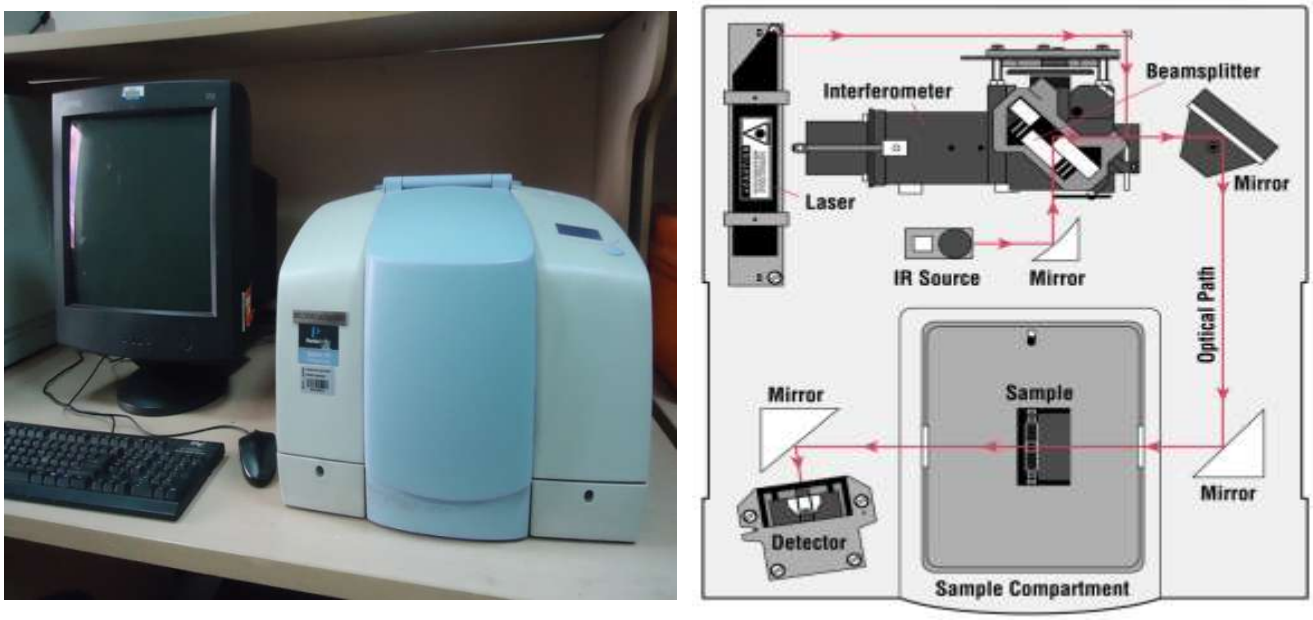

Figure 3.11 (a) FTIR Spectrometer (b) Schematic diagram of FTIR [67]

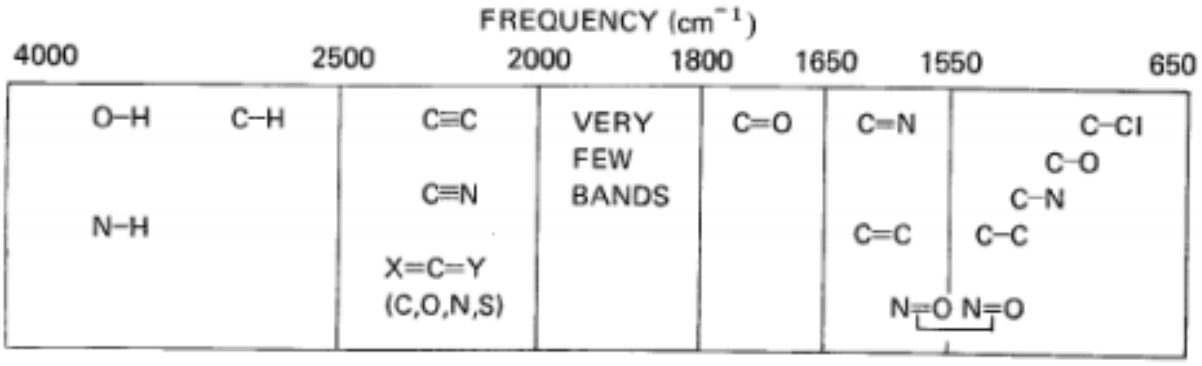

Figure 3.12 IR-absorption regions for various types of bonds [68]

3.4.6 Cyclic Voltammetry (CV)

Cyclic Voltammetry is the most commonly used method to obtain quantitative data for electrochemical reactions. It provides data for redox processes, adsorption processes and for heterogeneous electron transfer reactions. It also determines the values of redox potentials for electro-active species. Using CV, information about the type of reactions and the potentials at which they occur can be obtained easily. This method is helpful in terms of chemical analysis, capacitors, and investigations on batteries.

Cyclic Voltammetry, measures the current in response to the application of a triangular shape voltage to the electrode in an unagitated solution [68]. During the voltage sweep, the potentiostat measures the current that produces as a result of electrochemical reactions taking place at the electrode-electrolyte interface and consecutive to the applied voltage. The shape of the obtained curves and their behavior towards the function of triangular wave frequency, provide elementary information about oxidation reduction reactions

The cyclic voltammograms is a plot in which current response is plotted as a function of the applied voltage. Conventionally, this technique is implemented using an analog ramp. Because of the digital nature of the potentiostat, the actual ramp is applied such that it consists of a series of small voltage steps that estimates the desired linear ramp.

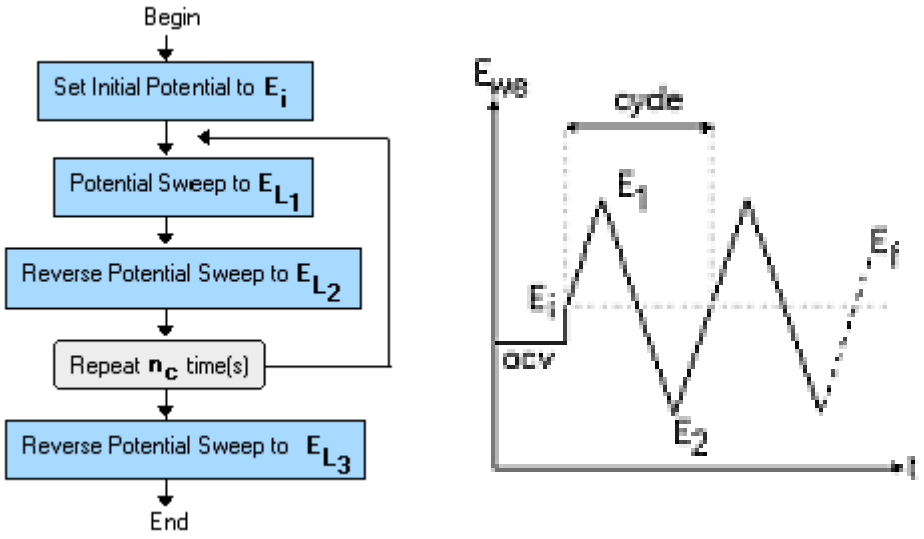

Figure 3.13 (a) General schematic for CV (b) CV graphic representation

Figure 3.13(a) explains the basic steps used for CV in EC lab software. It starts by setting an initial potential value E_i, then defining 1st potential sweep with a final limit E1 and 2nd potential sweep with final limit E2. Then the user can repeat 1st and 2nd potential sweeps for "n" times. Finally a last condition scan reverse to the previous one is executed with its own limit E_f. 3.13(b) shows the potential sweep is applied in the form of a digital potential staircase *i.e.* it runs defined potential increments at regular intervals of time. The software regulates the potential increments to be as small as possible. Figure 3.14 represents the detailed column diagram for the Cyclic Voltammetry.

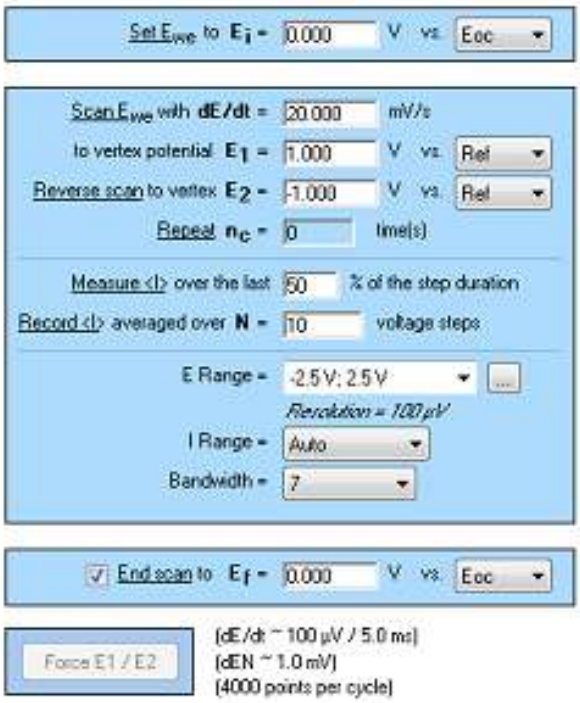

Figure 3.14 Detailed column diagram of Cyclic Voltammetry

In the present work, the electrochemical behavior of the supercapacitor was characterized through Cyclic Voltammetry using a multi-potentiostat/galvanostat (BioLogic VSP system) shown in figure 3.15 Cyclic voltammograms were recorded between –0.1 mV and +1.0 V at scan rate 50 mV and 100 mV. All experiments were conducted at room temperature (~298 K)

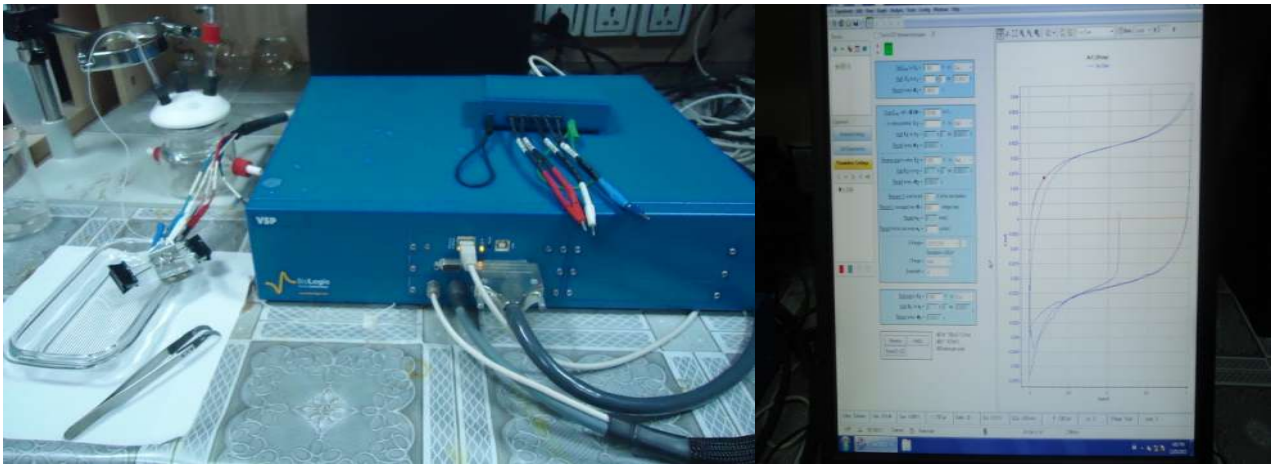

Figure 3.15 Diagram of Cyclic Voltammetry system

Chapter 4

4 Experimental work

4.1 Preparation of Graphene Oxide (GO)

Graphene oxide (GO) was prepared by following a simple room-temperature preparation technique that was reported for the production of high-yield, large-area GO [9].

4.1.1 Simplified Hummer's Method

To convert graphite flakes into GO, H_2SO_4 and H_3PO_4 in 9:1 ratio (120:13) ml were mixed in a round bottom flask under constant magnetic stirring. Graphite flakes (1 g) were added under magnetic stirring into pre-mixed acids. In the end $KMnO_4$ (3 g) was added very slowly, crystal by crystal, into the mixture under constant magnetic stirring of 400 rpm. Initially mixing was carried out under room temperature, no heating was used, but due to the addition of $KMnO_4$ into the mixture temperature of the solution was raised to 50 ^oC indicating exothermic nature of the reaction. One pot blend was stirred for three days (400 rpm) at room temperature. After three days the mixture colour transformed from purplish green to grayish brown. To stop the oxidation reaction 30% H_2O_2 (5 ml) was poured into the reaction mixture which turned the mixture into bright yellow colour. 30% H_2O_2 reduces the permanganate and manganese dioxide into manganese sulfate.

4.1.2 Washing and workup

To remove the metal impurities the mixture was washed repeatedly through centrifugation at 4000 rpm(30 min each time) with 1M HCl and DI water until its pH=7. The filtrate was centrifuged at 4000 rpm and the supernatant decanted away. During the washing process with deionized water, the graphite oxide experienced exfoliation when washed with DI water. As a result the graphene solution thickened and GO gel was formed in the described process [9].

Figure 4.1 GO after washing and work up

4.1.3 Exfoliation of graphite oxide into graphene oxide (GO)

A mild sonication (80 W, 5 min) was employed to exfoliate graphite oxide into GO and homogeneous GO suspension was obtained.

4.1.4 Drying of the GO gel

A small portion of the GO gel (10 ml) was taken from the main suspension and vacuum dried at 40 ^{o}C for 24 hrs to completely remove water residues. Dried flakes were weighed using very sensitive microbalance (resolution 0.1 mg). Weight of the dried flakes was 14.86 mg giving an estimate of concentration of suspension 1.5 mg/ml, which was used in calculations for establishing next experimentation. The dried powder itself was used for FTIR and XRD characterization of Graphene oxide.

4.2 Functionalization of the Graphene oxide

Functionalization can be accomplished in two ways. Either covalently attach external atoms directly with the carbon of graphene that leads to the tuning of electronic structure and formation of defect sites or to covalently couple the native functional group of GO with the guest functional group. Along with diverse electrical properties compared to undoped graphene, increased thermal stability and mechanical strength is also achieved as a result of functionalization [30]. Graphene oxide was coupled with Levofloxacin. Levofloxacin (LOF) is an antimicrobial agent [69] with molecular formula $C_{18}H_{20}FN_3O_4$.

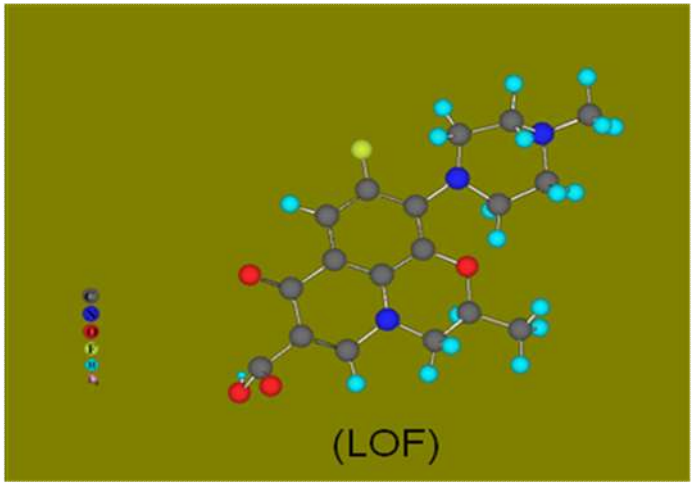

Figure 4.2 Ball and stick model of levofloxacin molecule

In the present work, different experiments were performed for the successful covalent functionalization of Graphene oxide.

4.2.1 Covalent Functionalization

Levofloxacin was covalently coupled onto the surface of Graphene Oxide through Steglich esterification, which was catalyzed by DCC and DMAP [70].

Esterification reaction represents a chemical reaction in which two participants react and (in general an alcohol and an acid) forms an ester. In our case we wanted the coupling of GO with LOF by the esterification reaction between the hydroxyl and carboxylic groups of GO and LOF (in the presence of DCC and DMAP) respectively.

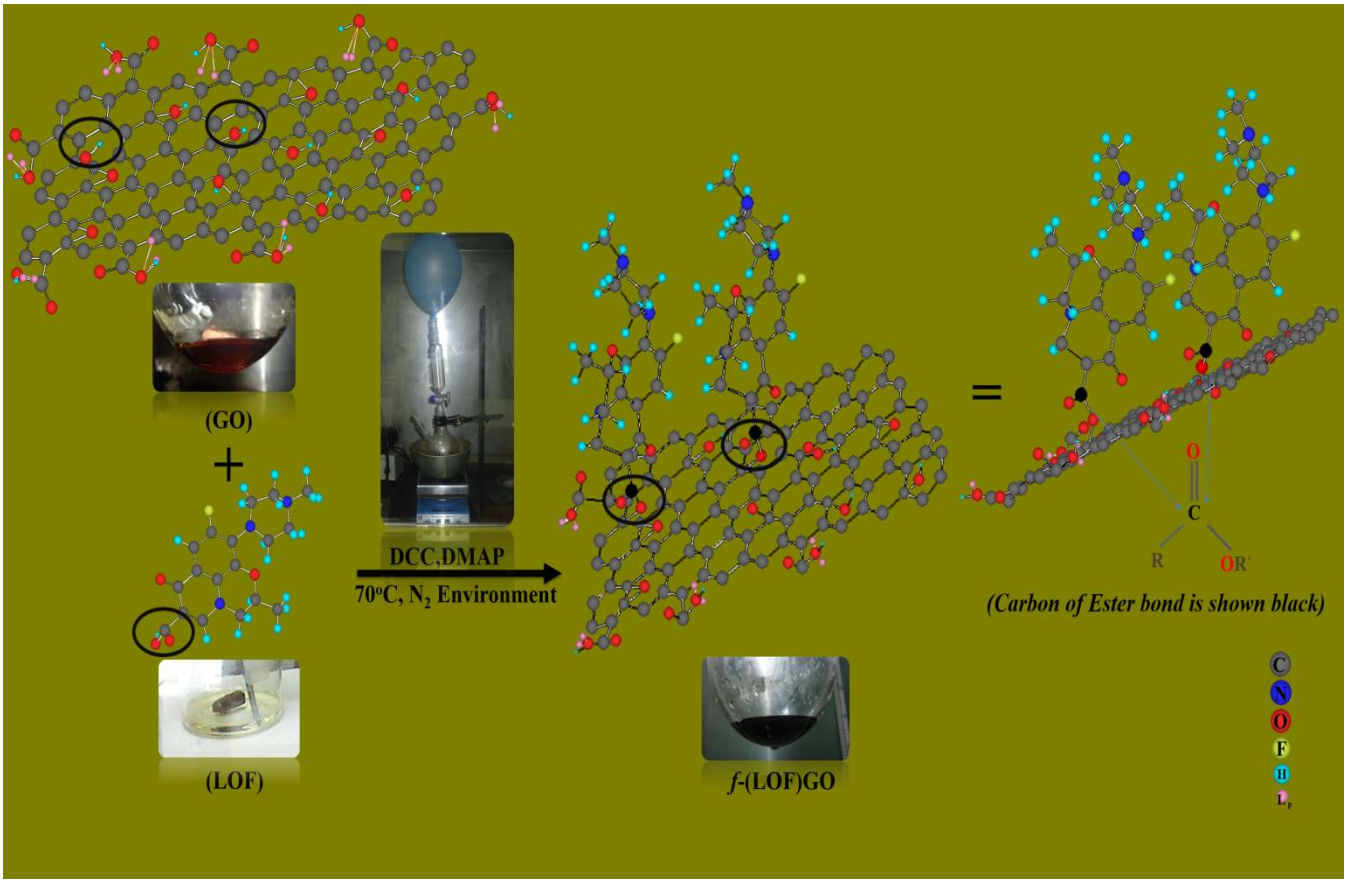

Figure 4.3 Illustration of the covalent-functionalization of GO

General Synthetic Protocol

Following protocol was used for the functionalization of GO with LOF using esterification reaction as presented in figure 3.

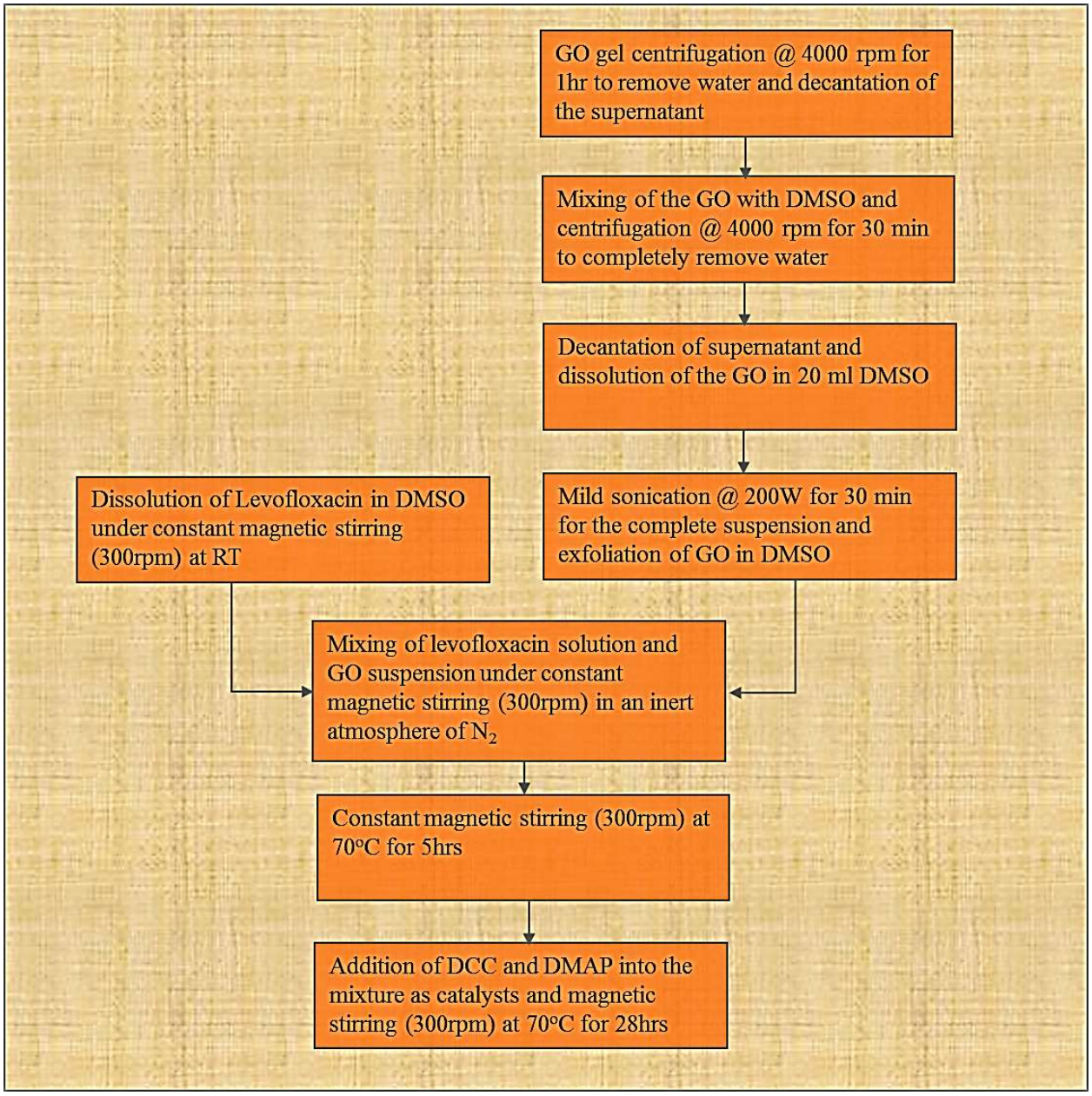

Figure 4.4 Synthesis protocol for the covalent functionalization of GO

Experimental details

Dissolution of Levofloxacin

Dimethyl sulfoxide (DMSO) was used as a solvent for LOF which is miscible with water along with its property to dissolve drugs where LOF is soluble up to 100 mM. To prepare a homogenous solution of the compound, 180 mg of LOF was dissolved in 20 ml DMSO. The resulting solution (25 mM) was stirred at 300 rpm for half an hour at room temperature in a glove box under an inert environment of N_2.

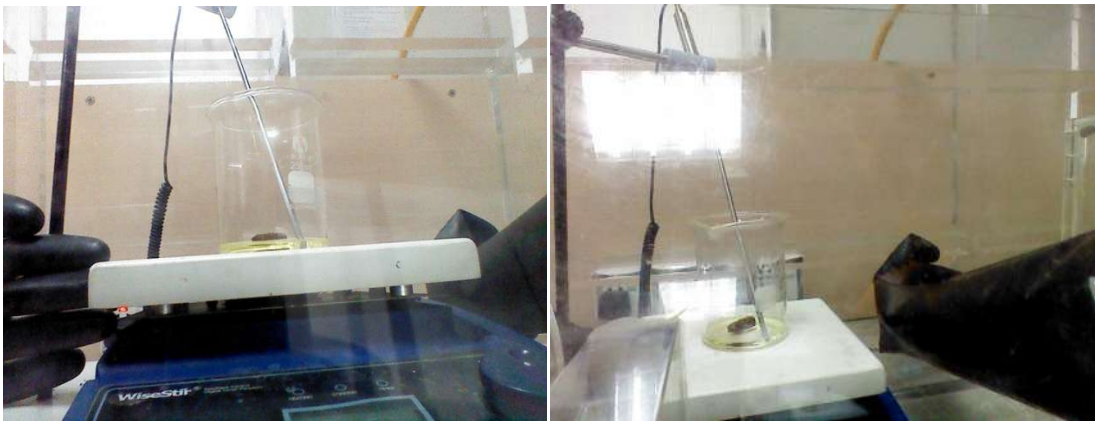

Figure 4.5 LOF solution in the glove box

Preparation of GO suspension in DMSO

12 ml GO gel conc. (1.5 mg/ml) was centrifuged at 4000 rpm for 2 hrs and water was decanted away. Then 10 ml DMSO was mixed with GO gel which resulted in the release of heat indicating an exothermic reaction. Since DMSO is miscible with water, after mixing of GO gel into DMSO centrifugation was performed (4000 rpm) for 90 min to remove water traces from GO gel and supernatant was decanted away. This step was repeated twice. Finally GO was stirred magnetically (150 rpm) in 20 ml DMSO for 10 min. The suspension was sonicated (200 W) for 30 min for exfoliation and formation of clear suspension of GO in DMSO.

Figure 4.6 (a) GO in DMSO before the sonication (b) GO in DMSO after the sonication in DMSO

Esterification reaction for the functionalization of GO with LOF

LOF/DMSO solution and GO/DMSO suspension was mixed under constant magnetic stirring (300 rpm) at room temperature under N_2 environment in a glove box. After 30 min temperature of the mixture was raised to 70 ^oC and magnetic stirring was continued for next 5 hrs at the same experimental conditions followed by the addition of DCC and DMAP as catalysts and stirring continued for another 28 hrs at 70 ^oC. Finally, the reaction product was cooled to room temperature and stirring continued for another 36 hrs.

Figure 4.7 Experimental set up for the functionalization of GO

Extraction of coupled product from the solution

To remove the solvent and excess drug, the solution was dried under high vacuum (10^{-6} Torr) for 24 hrs and the dried/functionalized Graphene oxide was obtained in the form of powder. The dried product was then used for the characterization purposes.

Figure 4.8 Reaction mixture at the start (a) and at the completion (b) of the reaction

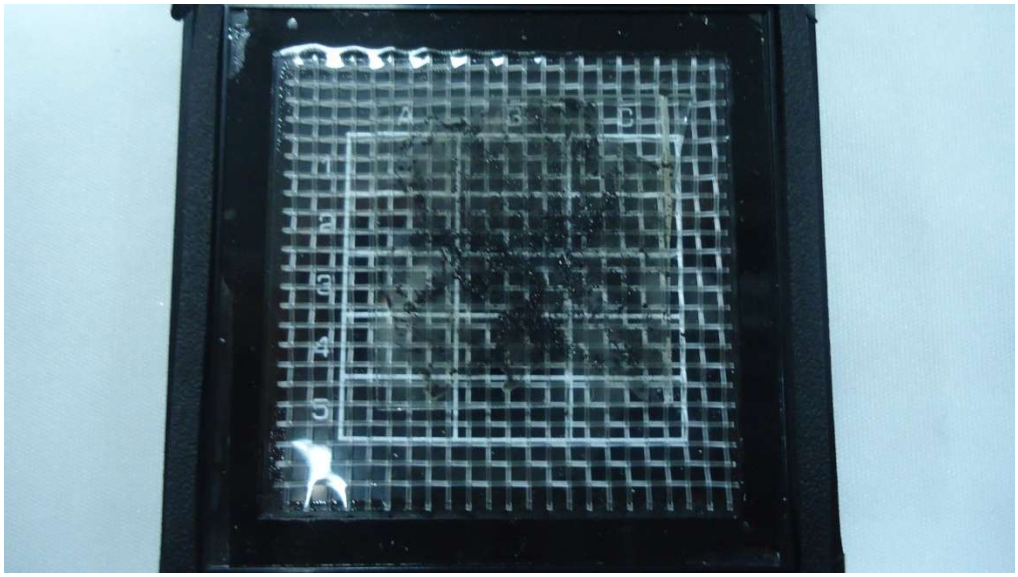

Figure 4.9 Vacuum dried product (f-(LOF)GO)

This experimental procedure was performed three times with different GO: LOF ratios and reaction parameters (given in Table 4.1 and Table 4.2)

Table 4.1 Relative conc. of reactants and catalysts

Experiment#	DMSO(ml)	LOF(mg)	GO(mg)	DCC(mg)	DMAP(mg)
GO_LOF_1	20	180	18	1100	70
GO_LOF_2	20	180	18	1100	70
GO_LOF_3	20	21	10	117	20

Table 4.2 Reaction parameters

Experiment#	Step #1:Stirring before addition of catalyst		Step #2:stirring after addition of catalyst		Step#3:Mixture cooling and stirring	
	Time(hrs)	Temp(^{o}C)	Time(hrs)	Temp(^{o}C)	Time(hrs)	Temp(^{o}C)
GO_LOF_1	5	70	28	95	36	RT
GO_LOF_2	1	95	12	95	48	RT
GO_LOF_3	1	70	36	70	48	RT

4.3 Preparation of Test Electrodes

GO and *f*-(LOF)GO were used as active materials for the Supercapacitor test electrodes. Aluminum (Al) was used as current collector and as substrate as well as for support purpose. Before using, Al-foil was cleaned with IPA and acetone subsequently then rinsed with DI water. For the electrode deposition , GO and *f*-(LOF)GO solutions were drop casted onto the Al-foil in a Petri dish and dried in an oven at 50 ^{o}C for 3 hrs.

Rectangular shape electrodes (25x10 mm^2) were cut to check the electrochemical response of the active material for supercapacitor applications and for surface morphology characterization with SEM and Optical microscope.

Figure 4.10 Electrodes with f-(LOF)GO drop casted and dried on Al-foil

4.4 Preparation of Lab scale Supercapacitor

Supercapacitor cell was prepared by stacking two similar test electrodes. They were separated by a filter paper which was soaked in 1 M Na_2SO_4 solution and this sandwich structure was placed between two glass slides. Opposite ends of the glass slides were clamped to make a unit cell for electrochemical measurements [56].

Figure 4.11 Laboratory scale supercapacitor in two electrode configuration

Chapter 5

Results and discussion

5.1 Characterization of Graphene Oxide (GO)

The X-ray diffraction (XRD) pattern of GO was obtained on a STOE Powder X-ray diffractometer θ-θ (operating voltage 40 kV and current 40mA) utilizing a scanning rate of 0.5° min^{-1} ranging from 5° to 80° (2θ) with Cu Kα radiation (λ = 1.5418 Å). Samples were prepared, for XRD analysis, by spin coating GO dispersion on clean glass substrate. The substrate was dried under a luminescent light lamp (100 W) at a working distance of 10 cm for 45 min.

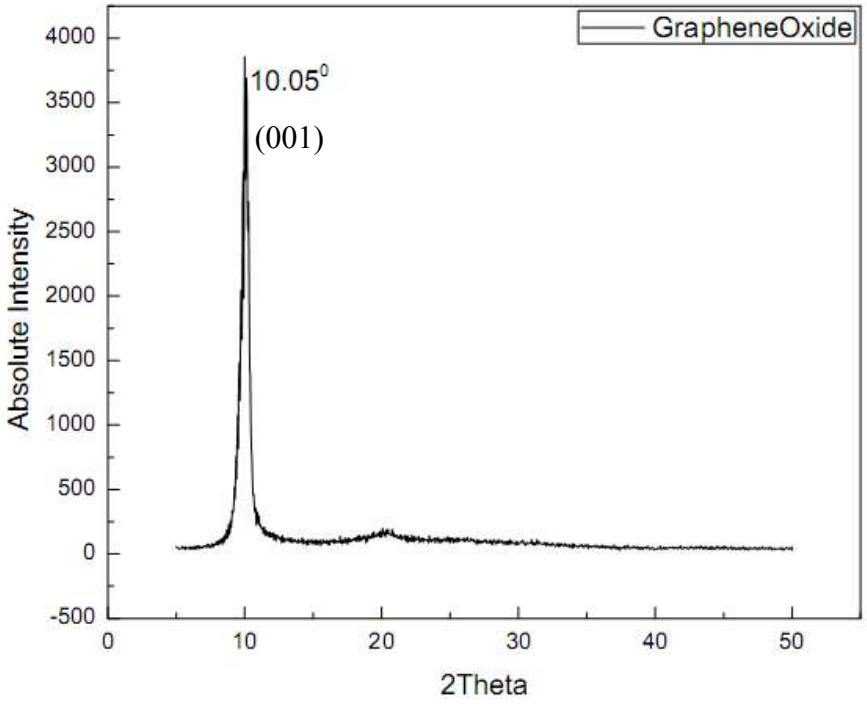

Figure 5.1 XRD spectrum of GO

Following parameters were deduced from the RAW data file by using X'Pert HighScore software.

Table 5.1 GO properties deduced from XRD data file by using X'Pert HighScore software

Pos. [°2Th.]	Height [cts]	FWHM [°2Th.]	d-spacing [Å]	Rel. Int. [%]	Tip width [°2Th.]
10.0502	2692.42	0.4320	8.79417	100.00	0.5184

XRD pattern in Figure 5.1 show a distinct diffraction peak (001) of GO at 10.05°. The interlayer spacing value (***d***) for GO is 0.87 nm has been calculated from the following Bragg`s law [71].

$$2dsin\theta = \lambda$$

The interplanar distance for carbon layers was found to be increased from 3.4 Å to 8.7 Å. This increase in the (***d***) for GO has been attributed to the inclusion of oxide functionalities on the carbon basal plane during the oxidation process [9]. The most intense peak for graphite at 2 θ = 26.4^{o} (corresponding to a d-spacing of 3.4 Å) is absent in this XRD pattern of GO sample which shows successful formation of GO.

UV measurements were recorded using a WPA Biowave II spectrophotometer (Biochrom, Cambridge, UK). Sample for the spectroscopy was prepared by making GO dispersion in DI water at a conc. of 0.5 mg/ml with the help of ultrasonication. Absorption spectrum was recorded in 1 mm quartz cuvette ranging from 200 to 300 nm.

UV measurements were utilized to examine the degree of oxidation for the GO suspensions. λ_{max} of the UV-Vis spectrum is used to reveal the degree of residual conjugation in both the pristine and functionalized GO. A higher λ_{max} in the spectrum represents that less energy has been used for the electronic transition which is an indication of the restoration of conjugation [14].

The spectrum in Figure 5.2 shows absorption peak of GO at 230 nm. The $\pi \rightarrow \pi^*$transitions of C-C , C=C bonds exist in the sp^2 hybrid areas of GO is the main cause for the appearance of this peak, as already described in the literature [72].

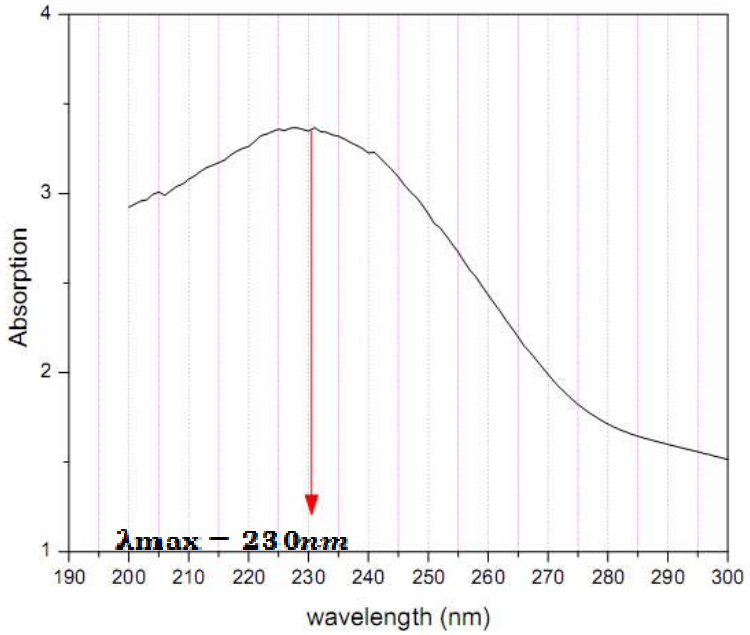

Figure 5.2 UV-Vis spectrum of GO

FTIR was used for the semi-quantitative analysis of chemically functionalized GO due to the sensitivity of IR to the creation as well as change of chemical bonds [30]. FT-IR provides a powerful tool to determine the presence of various oxygen functionalities in GO.

FT-IR spectra were recorded between 4000 and 400 $cm^{-1}$with 4 cm^{-1} resolution on a PerkinElmer spectrum 100 (FT-IR spectrometer), using a KBr disk method. Sample for FT-IR characterization was prepared by grinding vacuum dried GO flakes with KBr, while KBr was heated in an oven at 110 ^{o}C for 15 min. Then a 13 mm pellet was formed using this mixture in a manual hydraulic press at a pressure of 5 tons.

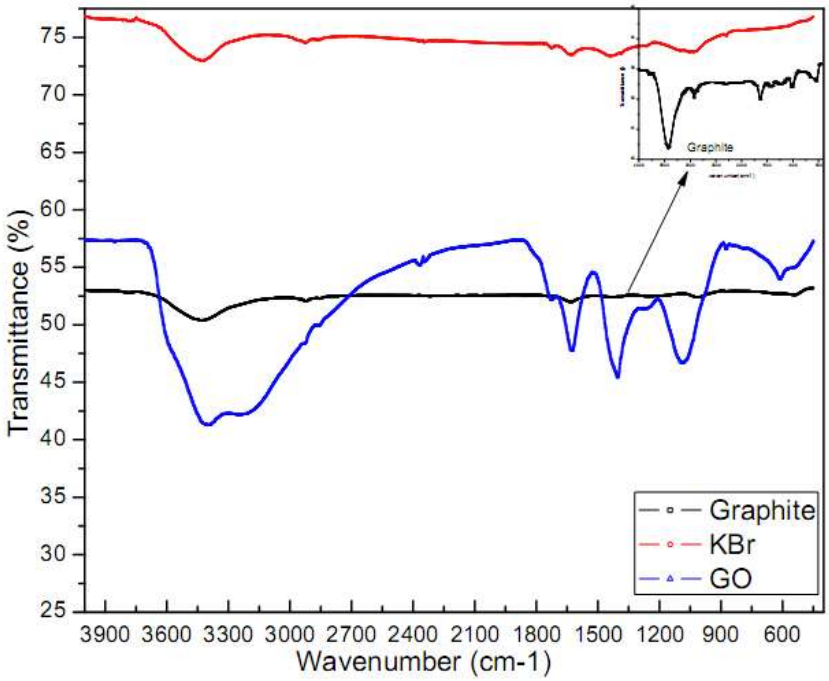

Figure 5.3 FTIR spectra of graphite and GO

Figure shows the FT-IR absorption spectra of graphite KBr, graphite and GO. In the graphite spectrum, the absorption bands at 3433 cm^{-1} was known to be the O-H stretching vibrations; the peak located at 1632 cm^{-1}could be attributed to the skeletal vibration of C=C from unoxidized sp^2 CC bonds [73]. After the oxidation reaction, the FT-IR spectra of GO apparently changed as compared to graphite. IR spectrum of GO shows the strong C=O stretching band at 1727 cm^{-1} [74]. The peak near 3398 cm^{-1} is due to the O-H stretching vibrations and the peak at 1626 cm^{-1} corresponds to the sp^2 character of C=C [75].The peaks at 1262 cm^{-1} and 1405 cm^{-1} are due to the epoxy C-O and C-OH vibrations respectively [73, 76]. FT-IR results indicated that oxygen-containing functional groups were established successfully onto the surface of graphite during the oxidation reaction.

The size and surface morphology of GO was studied with the help of SEM at the accelerating voltage (15 kV).GO dispersion at a conc. of 1mg/ml was prepared in DI water with the help of mild ultrasonication for 15 min. Then the dispersion was spin coated at 3000 rpm on a cleaned Si substrate. Sample was dried at room temperature. This Si piece was mounted on the Al sample holder with the help of carbon tape. SEM photographs were taken at different magnification in the range of 20 X to 5000 X using Nano NOVA FESEM. From these micrographs, it was established that the lateral measurements of GO varies between 1-10 µm. the light gray areas found on the substrate represents few layered GO sheets and dark gray areas represents multi-layered GO sheets. These micro-graphs showed very good exfoliation of GO sheets at the given conc.

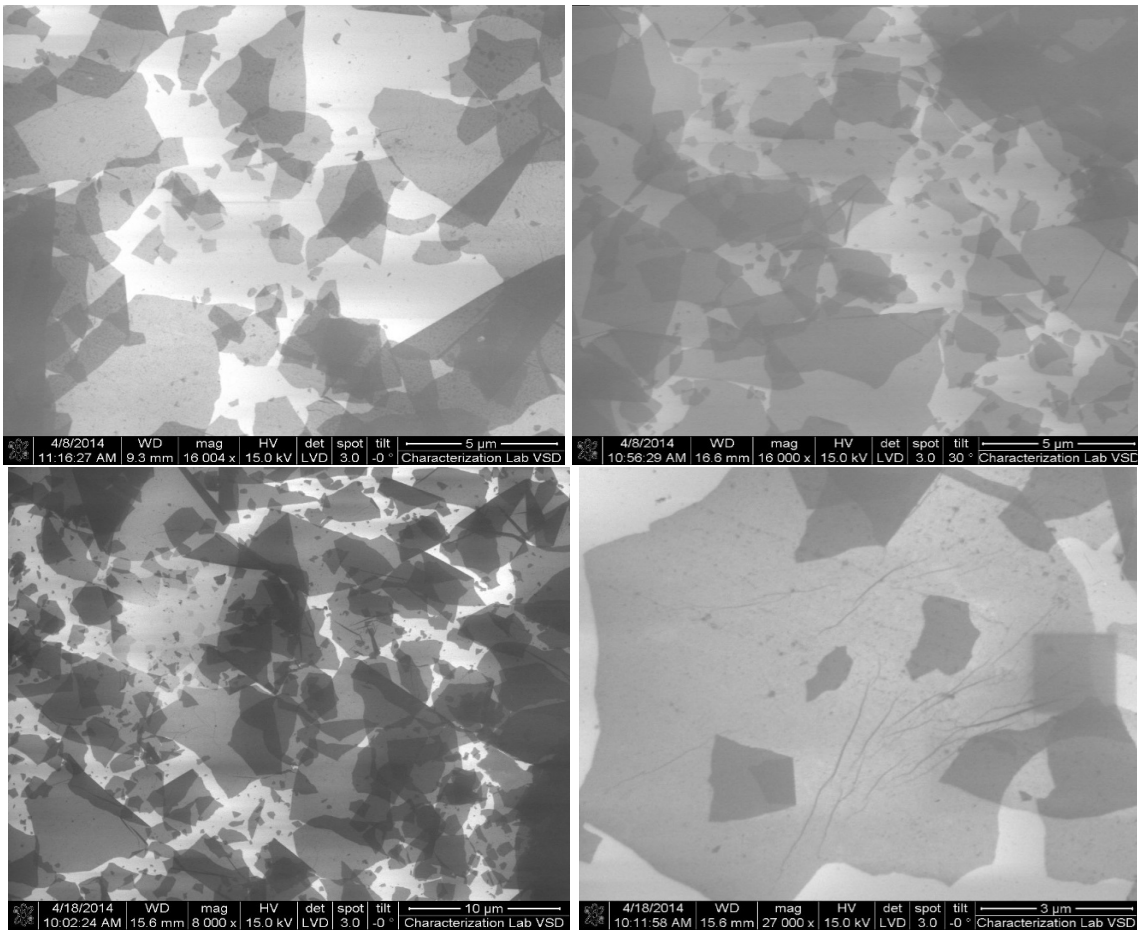

Figure 5.4 SEM micrographs of ex-foliated GO deposited on Si substrate

Graphite oxide flakes were deposited on several Si/Si_3N_4 substrates. By exploiting the hydrophilic behavior of GO, it was dispersed in water and then deposited onto a substrate using a drop-and-dry method. Since graphene sheets can be observed with the help of optical microscopy if these are deposited on the top of Si substrate having a thin layer of SiO_2 on its surface [77]. Graphene sheet's visibility strongly depends on the thickness of SiO_2 and wavelength of light as well. Figure 5.5 shows the graphene sheets deposited on the Si substrate having 300 nm thin layer of SiO_2. Since contrast is a quantitative parameter for the identification of number of graphene sheets on a substrate [77], it is estimated that light areas appeared in the optical images represents few layers of graphene sheets and relative darker areas indicate the presence of multilayer sheets.

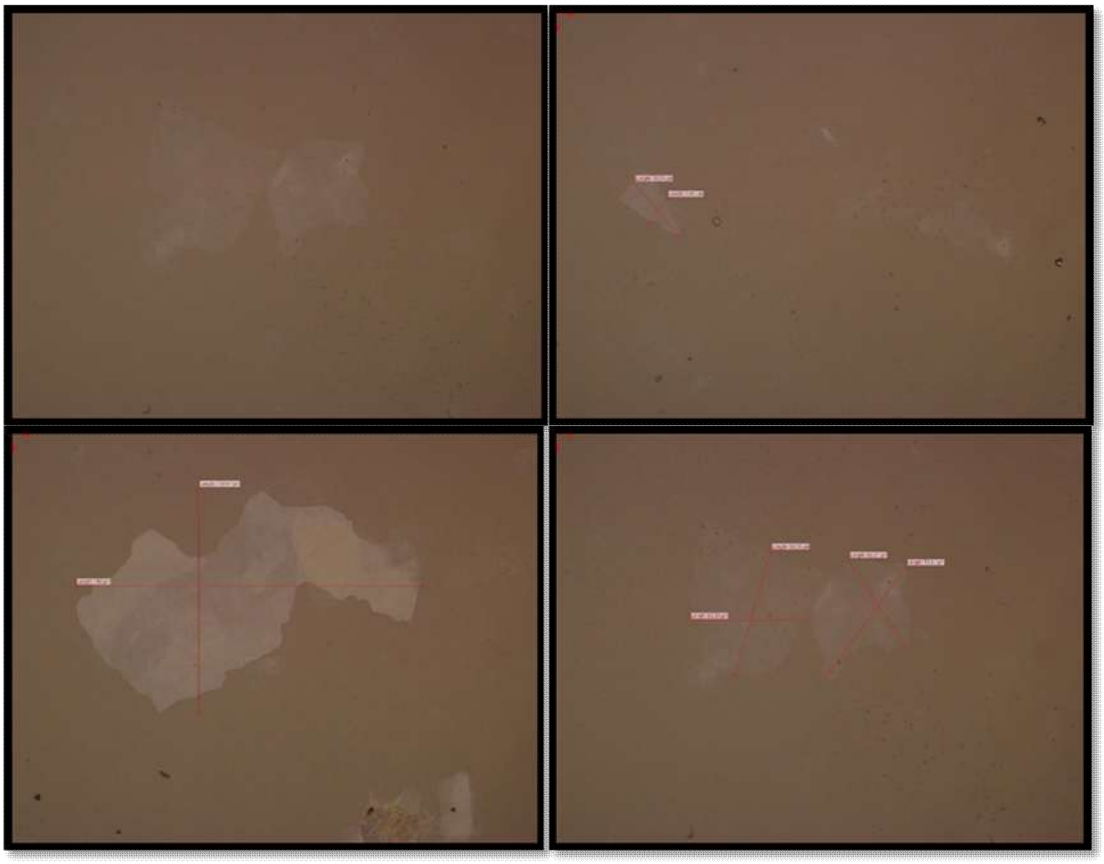

Figure 5.5 Optical images of GO deposited on SiO2/Si substrate

The size of these sheets ranges from 50 micron to 120 micron as shown in figures above.

pH dependent fluorescence of GO has been observed when GO (with acidic pH=3 during washing process) was deposited on Si substrates and observed through optical microscope as shown in Figure 5.6. It has been proposed that this effect arises due to the existence of electronic coupling of carboxylic functional groups (attached to the graphene periphery) with the adjacent carbon atoms of graphene [78]. Electron hole recombinations, taking place between conduction band bottom and neighboring localized states to the top of valence band, is the main reason behind this phenomenon [72]. Since these three types of functionalities (C-O, C=O and O=C-OH) contributed for the fluorescence hence these images also indicate the successful attachment of these functional groups during the oxidation reaction.

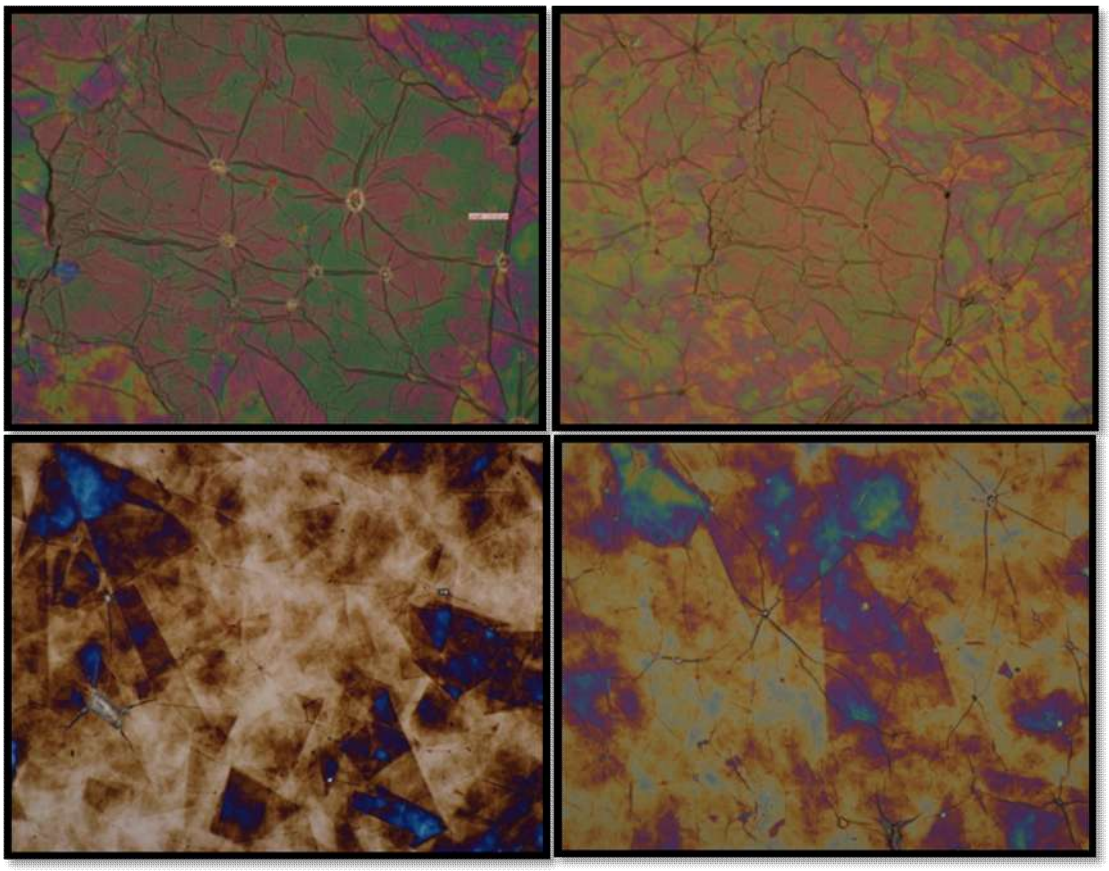

Figure 5.6 Optical images of GO deposited on SiO2/Si substrate

CV measurement is widely used to comprehend the electrochemical behavior of GO [30]. The electrochemical behavior of the electrochemical cell fabricated with GO was analyzed in 1M Na_2SO_4 solution in a two electrode configuration test cell.

The electrochemical performances supercapacitor electrodes of Al and GO coated Al have been investigated and their performances were compared. The CV curves of Al and GO-Al in Figure 5.7 depict an increase in CV current for the GO coated Al foil as compared to the bare Al as reported previously. CV curves exhibit quasi-rectangular shape without the presence of Faradic peaks which suggests the presence of double layer capacitance.

Capacitance of GO on Al electrode was determined by the division of current(mA) with scan rate(mV/s) of the CV curve, C=I/(dV/dt) [49]. CV studies were also performed from -0.1 mV to +1 mV at different scan rates. Figure 5.8 depicts the outcome of change in voltage scan rate on the electrode current (GO coated on Al-foil). At both scan rates shape of the CV curve is nearly same without any apparent distortion which illustrates admirable electronic and ionic transport inside the supercapacitor electrode material [79]. The calculated capacitance value for GO-Al and Al-foil is 0.522 mF and 0.0119 mF respectively.

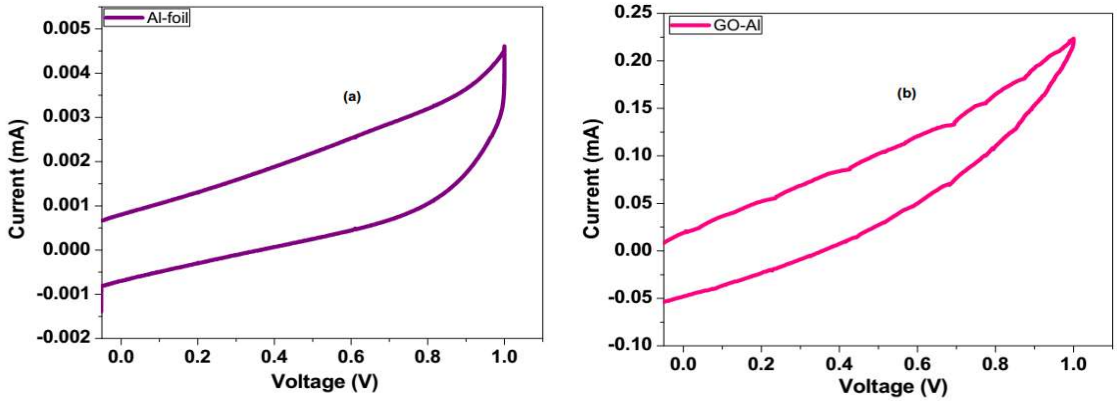

Figure 5.7 (a) CV curve of the supercapacitor with Al-foil as active electrode material (b) CV curve of the supercapacitor with GO coated on Al

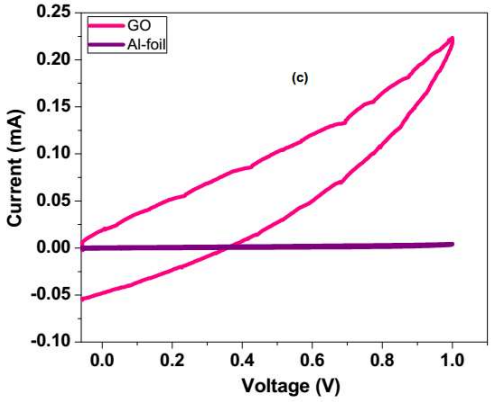

Figure 5.8 Effect of voltage scan rate for GO and Al-GO

5.2 Characterization of LOF

For the functionalization of GO, an organic compound Levofloxacin (LOF) was chosen due to the availability of the carboxylic groups in its structure. The crystalline structure of LVF was characterized by X-ray diffractogram as shown in figure 5.10, was in accordance with the reported literature [80].

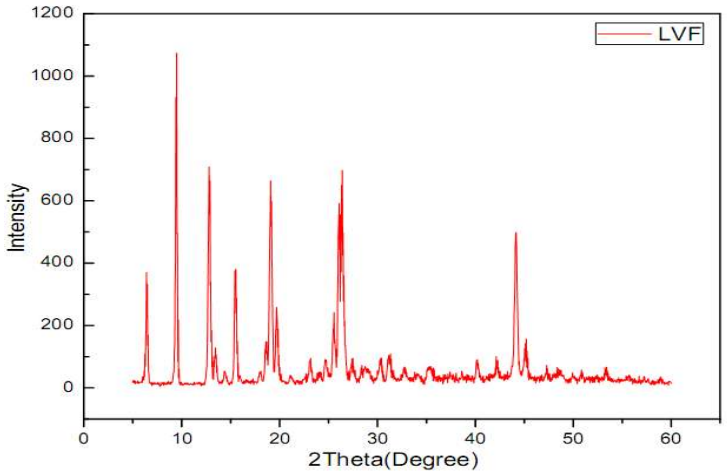

Figure 5.9 XRD spectrum of LOF

Sample for IR spectrum was prepared by mixing Levofloxacin powder with KBr, while KBr was heated in an oven at 110 ^{o}C for 15 min. Then a 13mm pellet was formed with this mixture in a manual hydraulic press at a pressure of 5 tons. Figure 5.11 shows the IR spectrum of LOF with major peaks at about 559, 581, 650,745.1, 802, 838.67, 873, 929, 977, 1027, 1084, 1193, 1242, 1292, 1305.0, 1333, 1517,1621, 1727, 2797, 3080 and 3262 cm^{-1} etc. as reported previously [81].

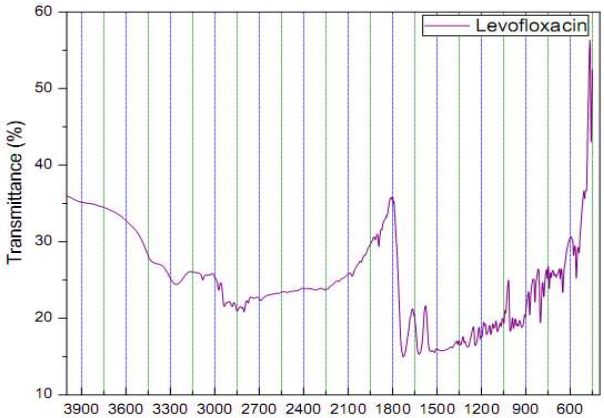

Figure 5.10 IR-spectrum of LOF

5.3 Characterization of Reduced GO (rGO)

During the reduction of GO with hydrazine hydrate, rGO sheets started agglomeration and the yellow-brown solution progressively created a black precipitates. XRD scan was run on the rGO clusters in the powder form. Reduction of GO was verified by the recurrence of the diffraction peak (002) at 24.5^0 and disappearance of the diffraction peak at 10.05° in the XRD graph.

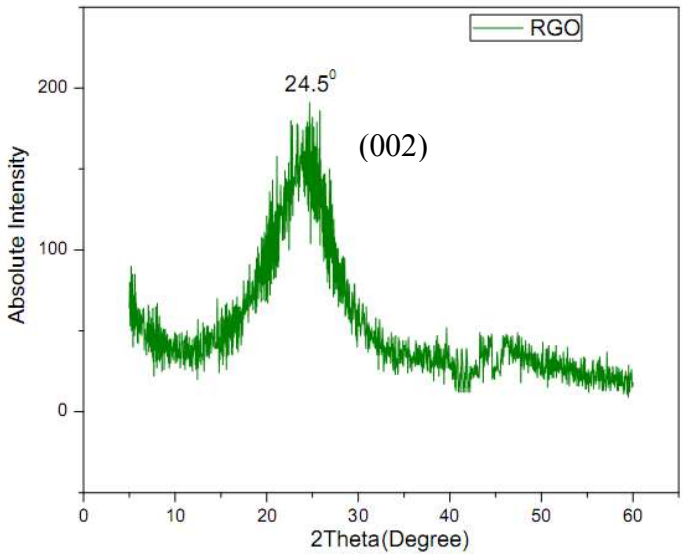

Figure 5.11 XRD profile of rGO

Chemical reduction of GO with hydrazine hydrate was also verified by FT-IR analysis of rGO powder obtained after the precipitation. Figure 5.13 shows the IR graphs of GO and rGO, clearly demonstrating the removal of OH, C-O and C=O functional groups as indicated by the decrease in the intensity of absorbance bands at the 3400 cm^{-1}, 1404 cm^{-1}, 1727 cm^{-1}.

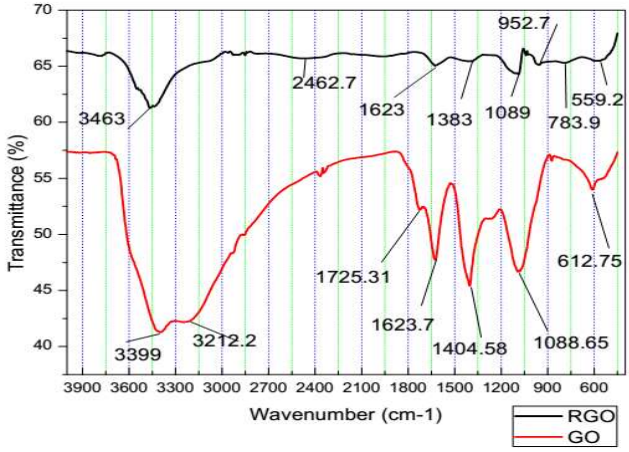

Figure 5.12 FT-IR spectra of GO and reduced GO

5.4 Characterization of Covalently Functionalized GO (*f*-(LOF)GO)

XRD scans were executed on different forms of the functionalized product *f*-(LOF)GO. After the functionalization reaction, when the coupled product was drop casted on the glass slide without removing excess LOF and diffraction pattern was obtained, the XRD pattern in Figure 5.14(d) contains some peaks of LOF along with the shift in the characteristic peak of GO from 10.5^{o} to 26.5^{o}. After recovering graphene through solution processing and vacuum drying a broader diffraction peak was observed at 24^{o} in Figure 5.14(c), which is attributed to reduction of GO and associated with large variation in the crystal size. This result is in agreement with the previous results [82-84]. This XRD profile clearly indicates coupling as well as reduction of GO evident from the absence of the 10.5^{o} peak, associated with the graphene oxide [9].

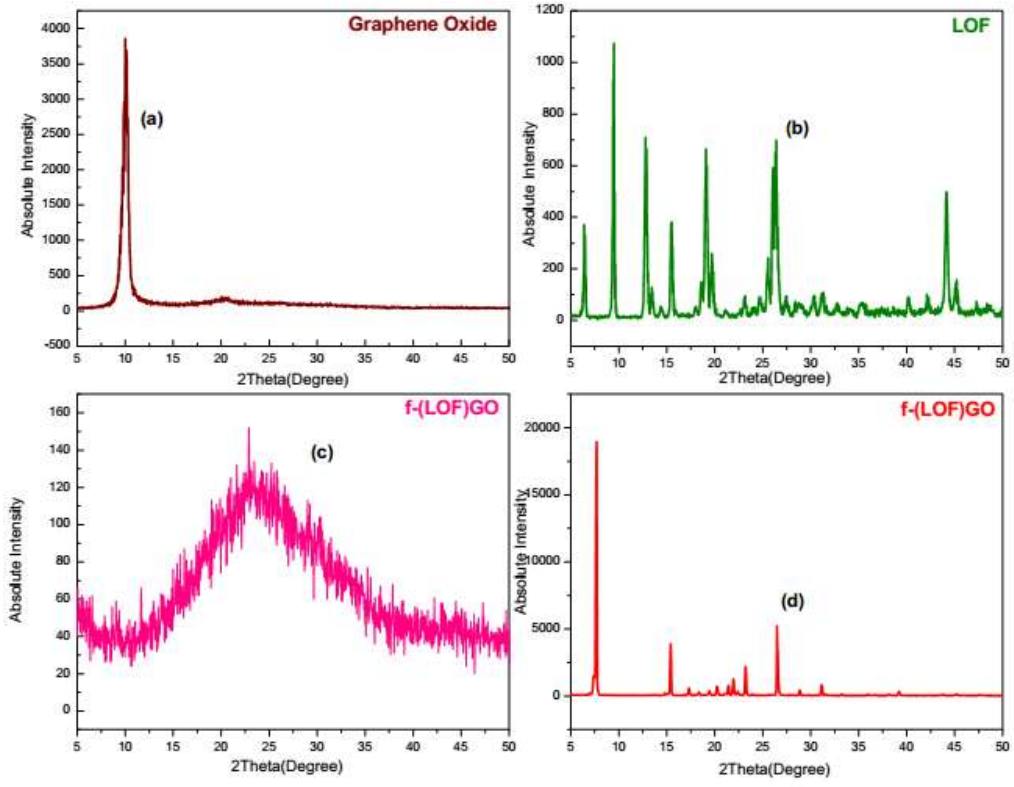

Figure 5.13 XRD patterns of (a) Graphene oxide (b) LOF (c) *f*-(LOF)GO vacuum dried (d) *f*-(LOF)GO drop casted

In order to further confirm the covalent attachment of LOF on the surface of GO sheets, UV measurements were performed. UV-Vis spectra were recorded for the product obtained after functionalization experiment. The dried functionalized GO (*f*-(LOF)GO) was sonicated in D.I water to obtain a stable suspension (at a conc. of 0.5 mg/ml) and the absorption spectrum was recorded in 1 mm quartz cuvette ranging from 200 to 450 nm.

UV-Vis spectrum of pure LOF contains peak at 292 nm associated with the λ_{max} of LOF [85]. Results show that the spectrum of *f*-(LOF)GO appears to be different from GO. In figure 5.15(b) the UV-Vis spectrum of the coupled product shows that the peak of GO has been red shifted to 268 nm which is attributed to the reduction of GO and to the n-π^* transitions of C-O bonds as reported previously [86]. The 299 nm peak may corresponds to the λ_{max} of LOF with a bathochromic shift (7 nm) attributed to the aromatic interaction between LOF and rGO similar to the red shift in pyrene's intrinsic absorption peak [87] and the observation of bathochromic shift in its Soret band of the porphyrin [88].

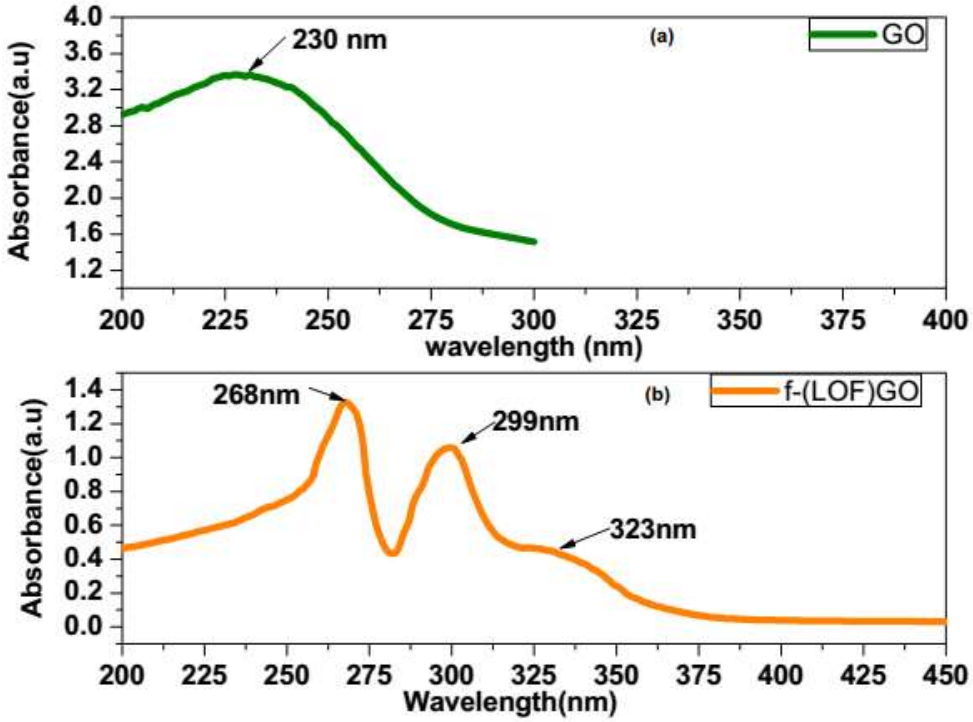

Figure 5.14 The UV-Vis spectra of (a) GO and (b) f-(LOF)GO

For the investigation on the presence of various functional groups on the coupled product, FTIR analysis was carried out. In Figure 5.16(c), the characteristic carboxyl C=O peak of LOF diminished and also intensity of the broad band corresponding to the O-H stretching vibrations is significantly reduced. Two new intense peaks appeared at 2853 cm^{-1} and 2923 cm^{-1} that represents symmetric and antisymmetric $=CH_2$ vibrations of graphene [89]. Moreover the peaks at 1650 cm^{-1} and 1207 cm^{-1} represents the formation of ester, indicating successful coupling of the LOF on the surface of GO through esterification reaction.

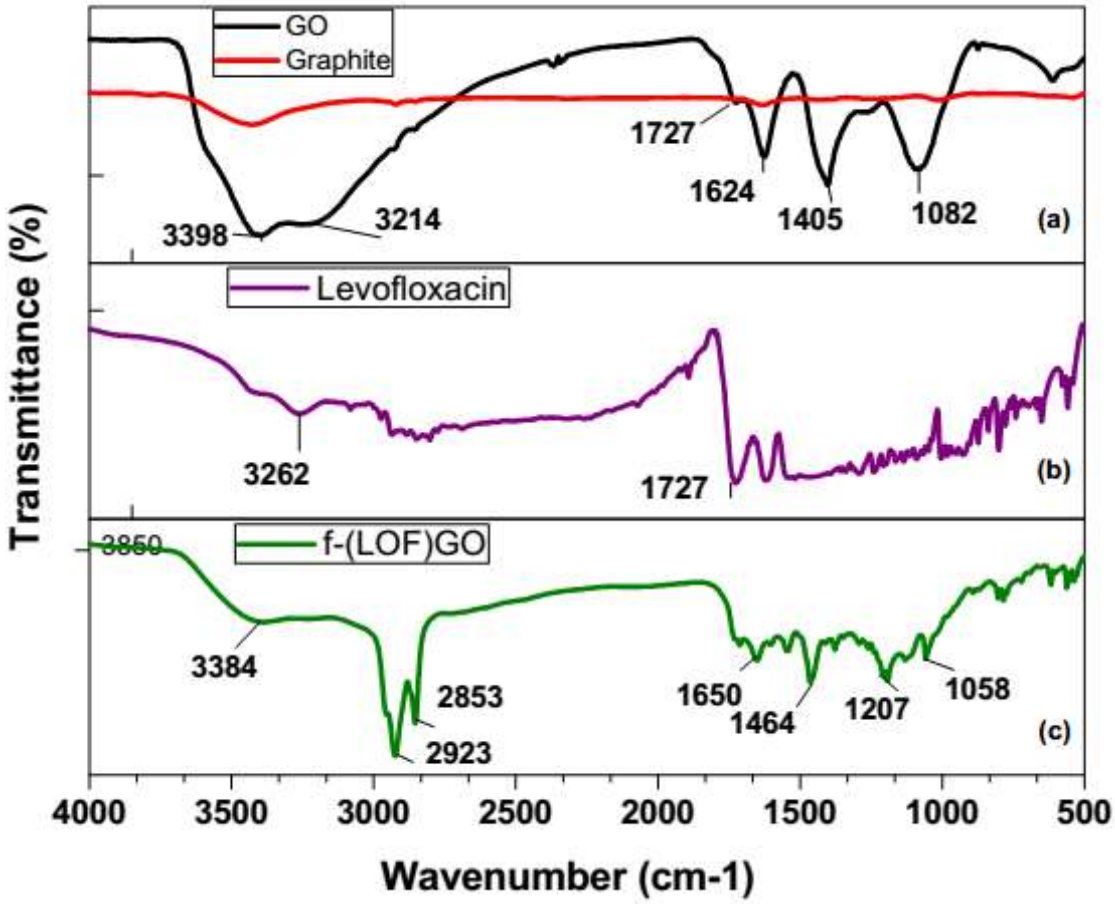

Figure 5.15 FTIR spectrum of (a) Graphite and GO, (b) LOF, (c) f-(LOF) GO

To investigate on the surface morphology of the coupled product, scanning electron microscopy (SEM) was carried out. Figure 5.17 (a,b) shows the SEM image of the functionalized *f*-(LOF)GO separated from the solvent by filtration and vacuum drying. Layered structure of the coupled product is visible in the magnified SEM image in Figure 5.17 (b).

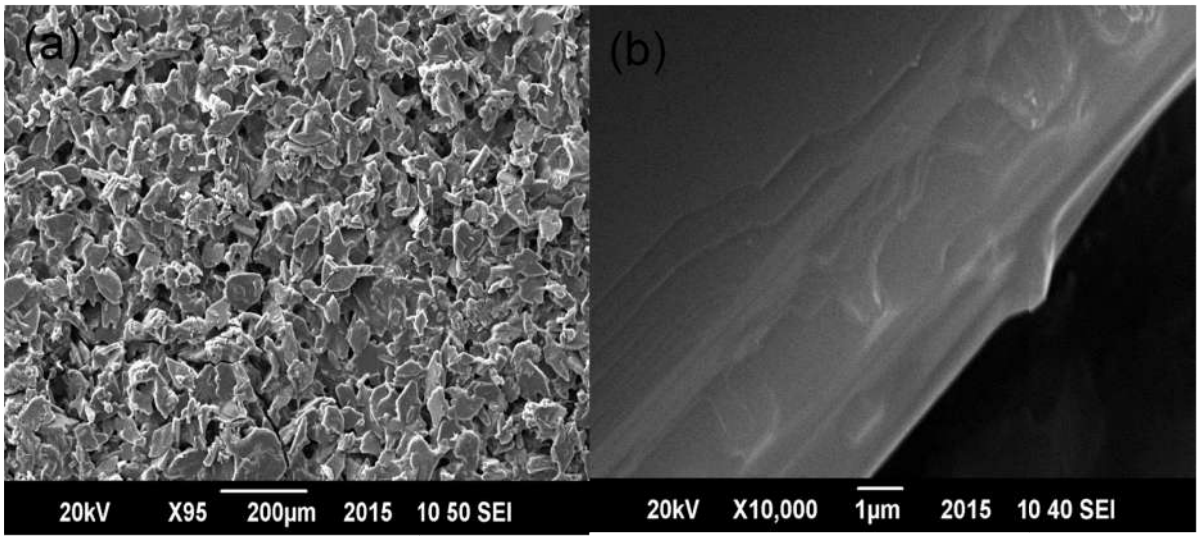

Figure 5.16 FESEM images of (a) vacuum dried f-(LOF)GO in powder form,(b) magnified image of *f*-(LOF)GO in (a)

Figure 5.18 (a-b) shows the micro-image of functionalized graphene extracted from the solvent with vacuum filtration. The cross-sectional image, as shown in Figure 5.18(d), displays the layer-by-layer stacking of the functionalized graphene sheets. Thickness of the coating was 6.3 µm. The cross-section of thin layer of *f*-(LOF) GO suggests that upon drying at 50 ^{o}C, DMSO-dispersed graphene sheets accumulated into layer-by-layer pattern. Table 5.2 shows the information obtained from the EDX spectrum showing the elemental composition of the coupled product which shows the presence of C, O, N and S. C and O are contributed by rGO while N indicated the coupling of LOF. C/O ratio in the EDX analysis indicates successful formation of the nano-hybrid as reported by others [90, 91]. The presence of sulfur is supposed to arise from the sulfuric acid used in the synthesis method for the preparation of graphene oxide [92].

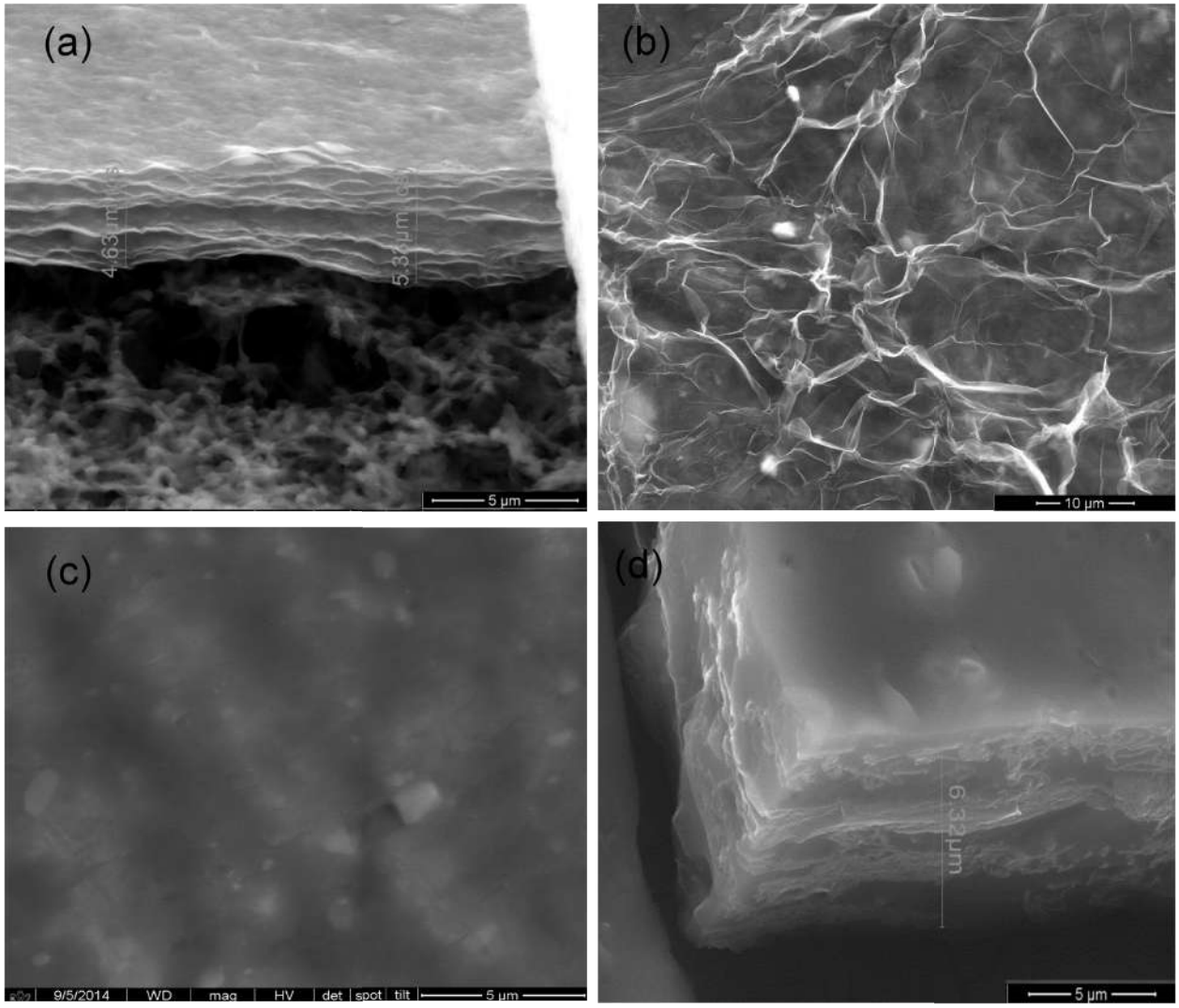

Figure 5.17 (a) cross-sectional view of vacuum filtered f-(LOF)GO (b) Topography image of f-(LOF)GO in (a), (c) topography of f-(LOF)GO coating on Al-foil, (d) cross-sectional view of f-(LOF)GO coating on Al-foil

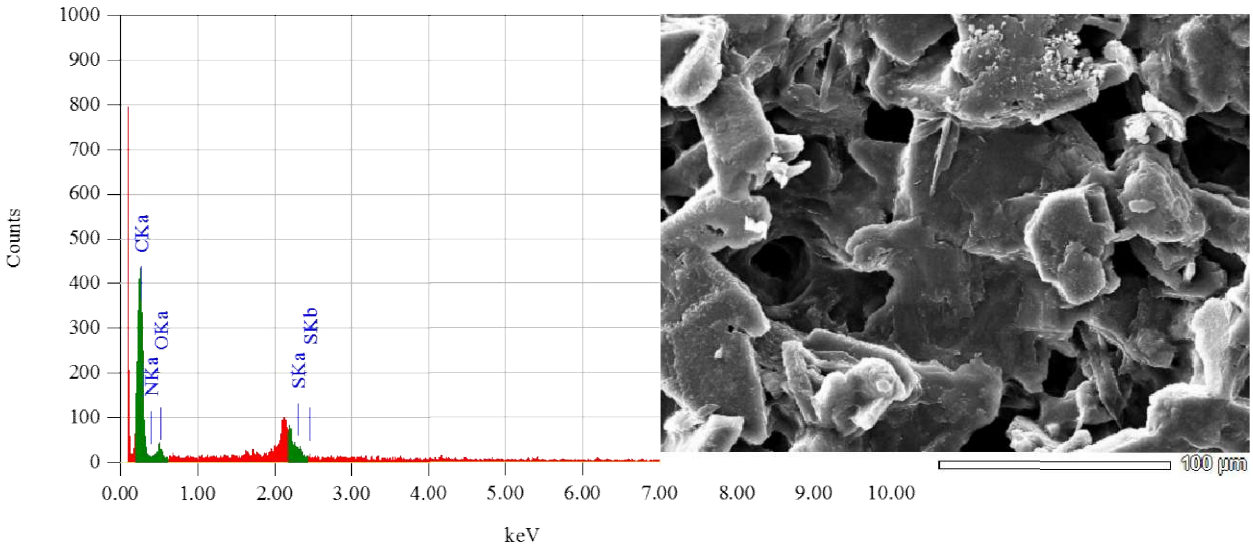

Figure 5.18 EDX spectrum of *f*-(LOF)GO and its SEM image

Table 5.2 Elemental analysis (EDX profile) of the functionalized graphene

ZAF Method Standardless Quantitative Analysis (Fitting Coefficient : 0.9101)				
Element	**(keV)**	**Mass %**	**Error %**	**Atom %**
C	0.277	37.01	0.35	41.58
N	0.392	44.90	5.80	43,26
O	0.525	17.85	5.79	15.06
S	2.307	0.24	0.66	0.10
Total		100.00		100.00

5.6 Effect of heating on capacitor electrode

To see the effect of heat on the morphology of the Supercapacitor electrode it was heated at 200 ^{o}C in a glove box under inert atmosphere and then its micrograph was taken in the SEM. The images in Figure 5.20 show that upon heating, coating of the coupled product from the Al-foil peeled off and several cracks developed in the deposited film. This phenomenon explains the loss in capacitance (depicted in CV graphs) of the electrodes due to loss in electrical contact between current collector Al-foil and the Supercapacitive layer of functionalized GO.

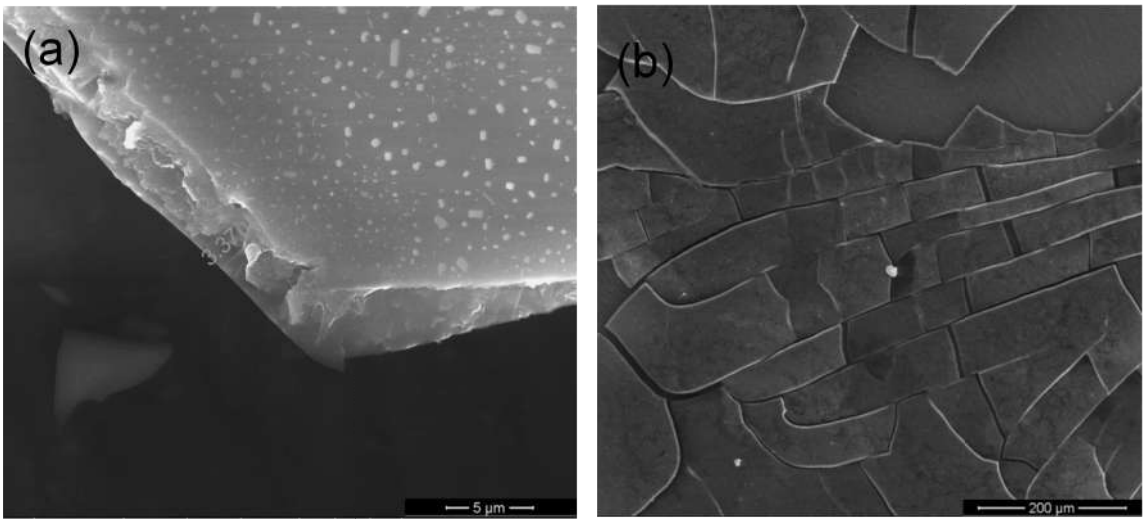

Figure 5.19 SEM micrographs showing (a) f-(LOF)GO coated Al-foil heated at 200 ^{0}C cross-sectional view (b) top view of f-(LOF)GO in (a)

5.7 Cyclic Voltammetry

The electrochemical behavior of the Supercapacitor with *f*-(LOF)GO coated electrode was characterized in 1M Na_2SO_4 solution using a Multi potentiostat/galvanostat (BioLogic VSP system). Cyclic Voltammetry shows that GO functionalized with LOF coated on Al-foil has good stability and improved capacitance as compared to the pristine GO coated on Al-foil

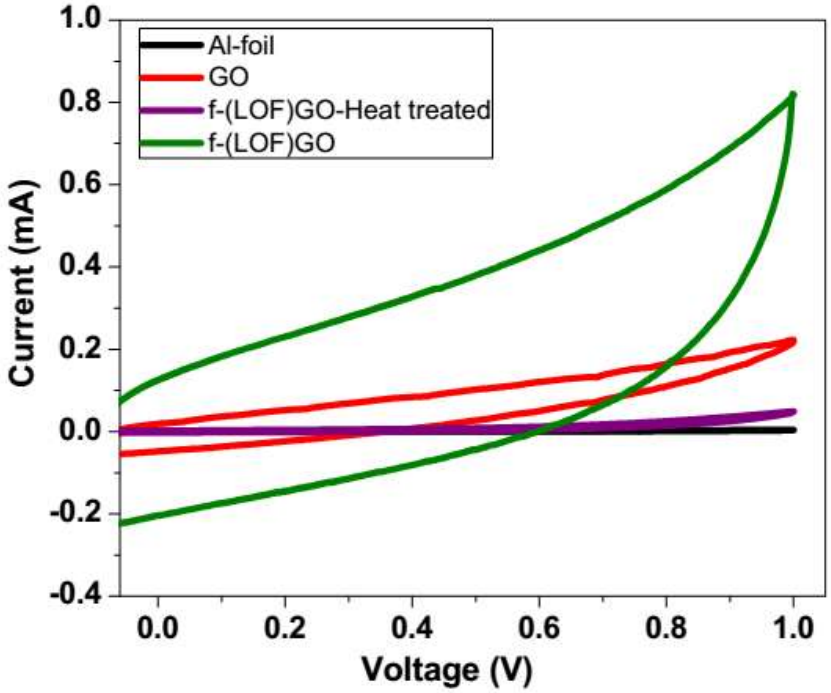

Figure 5.20 Cyclic voltammograms for Al-foil, GO and f-(LOF) GO and heat treated f-(LOF) GO at a scan rate of 100 mV/s

The CV curves of Al and GO-Al were used as a control and electrochemical behavior of *f*-(LOF)GO was investigated through Cyclic Voltammetry. CV curves exhibit quasi-rectangular shape without the presence of Faradic peaks which suggests the presence of double layer capacitance. Cyclic Voltammetry curves in Figure 5.21 show that *f*-(LOF)GO coated on Al-foil has larger value of current as compared to the pristine GO coated on Al-foil. However the supercapacitive electrode, coated with *f*-(LOF)GO and heat treated at 200 ^{o}C in a glove box under N_2, displays current even lower than the pristine GO. This decrease in the current is due to the fact that the coating of the functionalized graphene on Al-foil was cracked upon heating and

its electrical contact with Al-foil (current collector) was destroyed as evidenced by the SEM micrograph (Figure 5.20). Capacitance for GO and *f*-(LOF)GO was determined by the division of current(mA) with scan rate(mV/s) of the CV curves, C=I/(dV/dt) [49]. The capacitance of *f*-(LOF)GO_Al is 1.9 mF while the capacitance of GO-Al and Al-foil is 0.522 mF and 0.0119 mF respectively.

Specific capacitance

Specific capacitances of GO and *f*-(LOF)GO has been calculated by using the relation as described below [84].

$$C_{CV} = \frac{\int I\, dV}{(v \times \Delta V \times m)}$$

where

I = Capacitive current (A)

v = Voltage scan rate (V/sec)

ΔV= Potential window (V)

m= Mass of active material on single electrode

In our case

v = 0.1 V/sec

ΔV=1.1 V

m(GO)=20.8µg

m(*fGO*)=27.5µg

Integrated area of the CV curve for GO= 0.360 mAV

Integrated area of the CV curve for *f*-(LOF)GO = 0.078 mAV

$$C_{GO} = (0.078 \times 10^{-3})/(0.1 \times 1.1 \times 20.8 \times 10^{-6}) = 34\ F/g$$

$$C_{GO} = (0.360 \times 10^{-3})/(0.1 \times 1.1 \times 27.5 \times 10^{-6}) = 119\ F/g$$

The specific capacitance of the functionalized GO emerged to be nearly four times the specific capacitance of pristine GO.

Effect of variation in voltage scan rate

CV studies were for *f*-(LOF)GO based supercapacitor was also performed from -0.1 mV to +1.0 mV at different scan rates. Figure 5.22 depicts the result of change in voltage scan rate on the electrode currents of both pristine GO and functionalized GO. At both scan rates shape of the CV curve is nearly same without any apparent distortion which illustrates admirable electronic and ionic transport inside the supercapacitor electrode material [79].

Since specific capacitance of the *f*-(LOF) GO_Al was nearly four times the capacitance of GO which indicates the functionalization has significantly enhanced the electrochemical performance of GO. Moreover a higher current with increasing voltage scan rate justifies very good capacitive response for these electrodes.

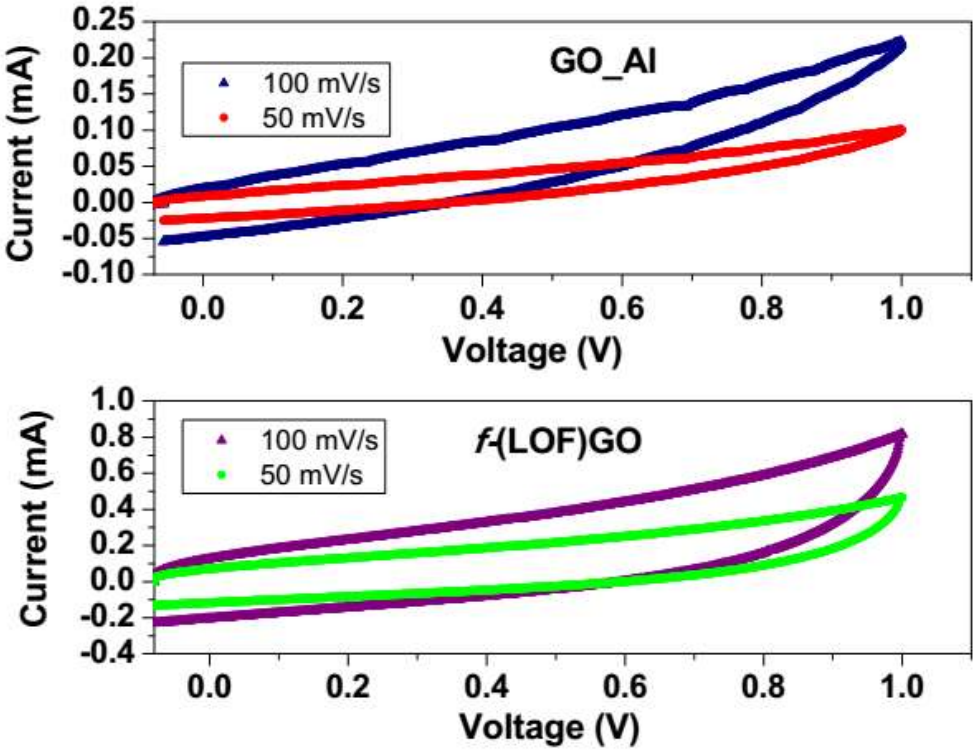

Figure 5.21 Cyclic voltammogram for GO and f-(LOF) GO at different scan rates

Conclusions

It is concluded that functionalized GO has improved the performance of EDLC supercapacitor. GO was prepared at room temperature by the oxidation of graphite flakes using improved Hummer's method. The covalently functionalized *f*-(LOF)GO was synthesized by esterification reaction. GO and *f*-(LOF)GO was characterized for structural, chemical, electrical, morphological and electrochemical properties. The electrochemical cell for supercapacitor was fabricated in two electrode configuration by drop casting and drying *f*-(LOF)GO on Al-foil.

XRD results of GO revealed the successful oxidation of graphite. SEM micrographs indicate the successful exfoliation of GO into single and few layered sheets. Optical images authenticated the exfoliation of GO into single and few layers. UV-Vis spectra showed the existence of absorption peak at 230 nm that corresponds to the extent of graphite oxidation. Absorption peaks in the FT-IR spectrum showed the occurrence of carbonyl, carboxyl and hydroxyl bonds on the surface of GO.

The XRD analysis of functionalize GO showed the attachment of LOF on the GO surface and its in-situ reduction. SEM showed the wrinkled morphology of the vacuum filtered functionalized GO sheets that implies its reduction into graphene sheets. C/O ration determined from the EDX results further validated the reduction behavior of GO. UV-Vis spectrum revealed the bathochromic shift of the absorption peak of GO and appearance of a new peak indicated the restoration of conjugation and attachment of LOF on GO surface. FT-IR spectrum of the functionalized GO demonstrated the elimination of carboxyl peak and appearance of ester peak which leads to the confirmation of the covalent coupling of LOF on GO.

Cross-sectional view in the SEM image of supercapacitor electrode showed the deposition and good adhesion of 6 micron thick film of active electrode material on the Al-current collector. Cyclic Voltammetry analysis was performed with both GO and *f*-(LOF)GO as active electrode materials for supercapacitor. CV curves exhibited quasi-rectangular shape without the presence of Faradic peaks which suggests the presence of double layer capacitance. The specific capacitance of *f*-(LOF)GO is 119 F/g while the capacitance of GO is 34 F/g. Specific capacitance of *f*-(LOF)GO is nearly four times the specific capacitance of GO which indicates the

functionalization has significantly enhanced the electrochemical performance of GO. At different scan rates shape of the CV curve is nearly same without any apparent distortion which illustrates admirable electronic and ionic transport inside the supercapacitor electrode material Moreover a higher current with increasing voltage scan rate justifies very good capacitive response for these electrodes**.**

In summary, the *f*-(LOF) GO has been successfully synthesized by esterification reaction which leads to functionalization and in-situ reduction process without using any toxic reducing agent. The coupled product was characterized by UV-Vis spectroscopy, XRD, FTIR, SEM and EDX to investigate the structure, morphology, functionalization and composition. All the results established the reduction as well as formation of *f*-(LOF) GO. Cyclic Voltammetry shows large current and greater area for *f*-(LOF) GO as compared to GO. Specific capacitance of the *f*-(LOF) GO was found to be nearly four times the specific capacitance of GO which indicates that the functionalization has significantly enhanced the electrochemical performance of GO.

References

[1] A.K. Geim, K.S. Novoselov, Nature materials, 6 (2007) 183-191.
[2] A. Fasolino, J. Los, M.I. Katsnelson, Nature materials, 6 (2007) 858-861.
[3] J.C. Meyer, A.K. Geim, M. Katsnelson, K. Novoselov, T. Booth, S. Roth, Nature, 446 (2007) 60-63.
[4] D.A. Brownson, D.K. Kampouris, C.E. Banks, Journal of Power Sources, 196 (2011) 4873-4885.
[5] O.C. Compton, S.T. Nguyen, small, 6 (2010) 711-723.
[6] Y. Zhu, S. Murali, W. Cai, X. Li, J.W. Suk, J.R. Potts, R.S. Ruoff, Advanced Materials, 22 (2010) 3906-3924.
[7] H. Kim, Y. Miura, C.W. Macosko, Chemistry of Materials, 22 (2010) 3441-3450.
[8] K.S. Novoselov, A.K. Geim, S. Morozov, D. Jiang, Y. Zhang, S.a. Dubonos, I. Grigorieva, A. Firsov, Science, 306 (2004) 666-669.
[9] N.M. Huang, H. Lim, C. Chia, M. Yarmo, M. Muhamad, International journal of nanomedicine, 6 (2011) 3443.
[10] P. Zhu, M. Shen, S. Xiao, D. Zhang, Physica B: Condensed Matter, 406 (2011) 498-502.
[11] B. Brodie, Ann. Chim. Phys, 59 (1860) e472.
[12] W.S. Hummers Jr, R.E. Offeman, Journal of the American Chemical Society, 80 (1958) 1339-1339.
[13] L. Staudenmaier, Berichte der deutschen chemischen Gesellschaft, 31 (1898) 1481-1487.
[14] D.C. Marcano, D.V. Kosynkin, J.M. Berlin, A. Sinitskii, Z. Sun, A. Slesarev, L.B. Alemany, W. Lu, J.M. Tour, ACS Nano, 4 (2010) 4806-4814.
[15] D.R. Dreyer, S. Park, C.W. Bielawski, R.S. Ruoff, Chemical Society Reviews, 39 (2010) 228-240.
[16] H. He, J. Klinowski, M. Forster, A. Lerf, Chemical Physics Letters, 287 (1998) 53-56.
[17] A. Lerf, H. He, M. Forster, J. Klinowski, The Journal of Physical Chemistry B, 102 (1998) 4477-4482.
[18] S. Mao, H. Pu, J. Chen, RSC Advances, 2 (2012) 2643-2662.
[19] S. Stankovich, D.A. Dikin, R.D. Piner, K.A. Kohlhaas, A. Kleinhammes, Y. Jia, Y. Wu, S.T. Nguyen, R.S. Ruoff, Carbon, 45 (2007) 1558-1565.
[20] Y. Si, E.T. Samulski, Nano Letters, 8 (2008) 1679-1682.
[21] H.C. Schniepp, J.-L. Li, M.J. McAllister, H. Sai, M. Herrera-Alonso, D.H. Adamson, R.K. Prud'homme, R. Car, D.A. Saville, I.A. Aksay, The Journal of Physical Chemistry B, 110 (2006) 8535-8539.
[22] I. Jung, D.A. Dikin, R.D. Piner, R.S. Ruoff, Nano Letters, 8 (2008) 4283-4287.
[23] H.A. Becerril, J. Mao, Z. Liu, R.M. Stoltenberg, Z. Bao, Y. Chen, ACS Nano, 2 (2008) 463-470.
[24] M.J. McAllister, J.-L. Li, D.H. Adamson, H.C. Schniepp, A.A. Abdala, J. Liu, M. Herrera-Alonso, D.L. Milius, R. Car, R.K. Prud'homme, Chemistry of Materials, 19 (2007) 4396-4404.
[25] G. Chen, W. Weng, D. Wu, C. Wu, J. Lu, P. Wang, X. Chen, Carbon, 42 (2004) 753-759.
[26] D. Yang, A. Velamakanni, G. Bozoklu, S. Park, M. Stoller, R.D. Piner, S. Stankovich, I. Jung, D.A. Field, C.A. Ventrice, Carbon, 47 (2009) 145-152.

[27] H. Chen, M.B. Müller, K.J. Gilmore, G.G. Wallace, D. Li, Adv. Mater, 20 (2008) 3557-3561.
[28] H.J. Shin, K.K. Kim, A. Benayad, S.M. Yoon, H.K. Park, I.S. Jung, M.H. Jin, H.K. Jeong, J.M. Kim, J.Y. Choi, Advanced Functional Materials, 19 (2009) 1987-1992.
[29] A. Furst, R.C. Berlo, S. Hooton, Chemical Reviews, 65 (1965) 51-68.
[30] Y. Hu, X. Sun, (2013).
[31] T. Kuila, P. Khanra, S. Bose, N.H. Kim, B.-C. Ku, B. Moon, J.H. Lee, Nanotechnology, 22 (2011) 305710.
[32] P. Laaksonen, M. Kainlauri, T. Laaksonen, A. Shchepetov, H. Jiang, J. Ahopelto, M.B. Linder, Angewandte Chemie International Edition, 49 (2010) 4946-4949.
[33] A.B. Bourlinos, D. Gournis, D. Petridis, T. Szabó, A. Szeri, I. Dékány, Langmuir, 19 (2003) 6050-6055.
[34] T. Kuila, S. Bose, C.E. Hong, M.E. Uddin, P. Khanra, N.H. Kim, J.H. Lee, Carbon, 49 (2011) 1033-1037.
[35] E. Bekyarova, M.E. Itkis, P. Ramesh, C. Berger, M. Sprinkle, W.A. de Heer, R.C. Haddon, Journal of the American Chemical Society, 131 (2009) 1336-1337.
[36] T. Kuila, S. Bose, A.K. Mishra, P. Khanra, N.H. Kim, J.H. Lee, Progress in Materials Science, 57 (2012) 1061-1105.
[37] S. Stankovich, R.D. Piner, S.T. Nguyen, R.S. Ruoff, Carbon, 44 (2006) 3342-3347.
[38] S. Stankovich, D.A. Dikin, G.H. Dommett, K.M. Kohlhaas, E.J. Zimney, E.A. Stach, R.D. Piner, S.T. Nguyen, R.S. Ruoff, Nature, 442 (2006) 282-286.
[39] J. Choi, K.-j. Kim, B. Kim, H. Lee, S. Kim, The Journal of Physical Chemistry C, 113 (2009) 9433-9435.
[40] M. Jayalakshmi, K. Balasubramanian, Int. J. Electrochem. Sci, 3 (2008) 1196-1217.
[41] E. Frackowiak, J. Machnikowski, F. Béguin, Novel Carbonaceous Materials for Application in the Electrochemical Supercapacitors, in: New Carbon Based Materials for Electrochemical Energy Storage Systems: Batteries, Supercapacitors and Fuel Cells, Springer, 2006, pp. 5-20.
[42] V. Subramanian, H. Zhu, R. Vajtai, P. Ajayan, B. Wei, The Journal of Physical Chemistry B, 109 (2005) 20207-20214.
[43] Y.-R. Nian, H. Teng, Journal of the Electrochemical Society, 149 (2002) A1008-A1014.
[44] E. Frackowiak, K. Metenier, V. Bertagna, F. Beguin, Applied Physics Letters, 77 (2000) 2421-2423.
[45] A. Laforgue, P. Simon, C. Sarrazin, J.-F. Fauvarque, Journal of Power Sources, 80 (1999) 142-148.
[46] A. Rudge, J. Davey, I. Raistrick, S. Gottesfeld, J.P. Ferraris, Journal of Power Sources, 47 (1994) 89-107.
[47] E. Frackowiak, F. Beguin, Carbon, 39 (2001) 937-950.
[48] R. Kötz, M. Carlen, Electrochimica Acta, 45 (2000) 2483-2498.
[49] M.D. Stoller, S. Park, Y. Zhu, J. An, R.S. Ruoff, Nano Letters, 8 (2008) 3498-3502.
[50] A.A. Balandin, S. Ghosh, W. Bao, I. Calizo, D. Teweldebrhan, F. Miao, C.N. Lau, Nano Letters, 8 (2008) 902-907.
[51] J. Xia, F. Chen, J. Li, N. Tao, Nature nanotechnology, 4 (2009) 505-509.
[52] P. Simon, Y. Gogotsi, Nature materials, 7 (2008) 845-854.
[53] J. Chen, B. Yao, C. Li, G. Shi, Carbon, 64 (2013) 225-229.
[54] C.-J. Shih, S. Lin, R. Sharma, M.S. Strano, D. Blankschtein, Langmuir, 28 (2011) 235-241.

[55] T. Chen, B. Zeng, J. Liu, J. Dong, X. Liu, Z. Wu, X. Yang, Z. Li, in: Journal of Physics: Conference Series, IOP Publishing, 2009, pp. 012051.
[56] F. Ban, S.R. Majid, N.M. Huang, H.N. Lim, International Journal of Electrochemical Science, 7 (2012).
[57] W.D. Callister, D.G. Rethwisch, Materials science and engineering: an introduction, Wiley New York, 2007.
[58] P. Lian, X. Zhu, S. Liang, Z. Li, W. Yang, H. Wang, Electrochimica Acta, 55 (2010) 3909-3914.
[59] Y. Waseda, E. Matsubara, K. Shinoda, X-ray diffraction crystallography: introduction, examples and solved problems, Springer Science & Business Media, 2011.
[60] D.K. Schroder, Semiconductor material and device characterization, John Wiley & Sons, 2006.
[61] J. Cazaux, Journal of microscopy, 217 (2005) 16-35.
[62] C.S. Kumar, UV-VIS and Photoluminescence Spectroscopy for Nanomaterials Characterization, Springer, 2013.
[63] H.-H. Perkampus, H.-C. Grinter, T. Threlfall, UV-VIS Spectroscopy and its Applications, Springer, 1992.
[64] B.C. Smith, (1999).
[65] D. Pavia, G. Lampman, G. Kriz, J. Vyvyan, Introduction to spectroscopy, Cengage Learning, 2008.
[66] B.C. Smith, Fundamentals of Fourier transform infrared spectroscopy, CRC press, 2011.
[67] E. FINAN, (2012).
[68] R.S. Nicholson, I. Shain, Analytical Chemistry, 36 (1964) 706-723.
[69] V. Niddam-Hildesheim, N. Gershon, E. Schwartz, in, Google Patents, 2008.
[70] J. Gao, F. Bao, L. Feng, K. Shen, Q. Zhu, D. Wang, T. Chen, R. Ma, C. Yan, RSC Advances, 1 (2011) 1737-1744.
[71] B.S. Murty, P. Shankar, B. Raj, B. Rath, J. Murday, Textbook of nanoscience and nanotechnology, Springer Science & Business Media, 2013.
[72] J. Shang, L. Ma, J. Li, W. Ai, T. Yu, G.G. Gurzadyan, Scientific reports, 2 (2012).
[73] Z. Liu, X. Duan, X. Zhou, G. Qian, J. Zhou, W. Yuan, Industrial & Engineering Chemistry Research, 53 (2013) 253-258.
[74] D. Liu, G. Huang, Y. Yu, Y. He, H. Zhang, H. Cui, Chemical Communications, 49 (2013) 9794-9796.
[75] P. Karthika, N. Rajalakshmi, K.S. Dhathathreyan, (2012).
[76] M.S. Diallo, Nanotechnology for Sustainable Development, Springer, 2014.
[77] P. Blake, E. Hill, A.C. Neto, K. Novoselov, D. Jiang, R. Yang, T. Booth, A. Geim, Applied Physics Letters, 91 (2007) 063124.
[78] C. Galande, A.D. Mohite, A.V. Naumov, W. Gao, L. Ci, A. Ajayan, H. Gao, A. Srivastava, R.B. Weisman, P.M. Ajayan, Scientific reports, 1 (2011).
[79] S. Biswas, L.T. Drzal, Chemistry of Materials, 22 (2010) 5667-5671.
[80] M. Reddy, S. Eswaraiah, K. Reddy, P. Prakash, in, Google Patents, 2004.
[81] M. Reddy, S. Eswaraiah, K. Reddy, P. Prakash, in, Google Patents, 2004.
[82] A.V. Murugan, T. Muraliganth, A. Manthiram, Chemistry of Materials, 21 (2009) 5004-5006.
[83] X. Xu, T. Wu, F. Xia, Y. Li, C. Zhang, L. Zhang, M. Chen, X. Li, L. Zhang, Y. Liu, J. Gao, Journal of Power Sources, 266 (2014) 282-290.

[84] Z. Bo, X. Shuai, S. Mao, H. Yang, J. Qian, J. Chen, J. Yan, K. Cen, Scientific Reports, 4 (2014) 4684.
[85] M. Cicuéndez, I. Izquierdo-Barba, M.T. Portolés, M. Vallet-Regí, European Journal of Pharmaceutics and Biopharmaceutics, 84 (2013) 115-124.
[86] F.T. Thema, M.J. Moloto, E.D. Dikio, N.N. Nyangiwe, L. Kotsedi, M. Maaza, M. Khenfouch, Journal of Chemistry, 2013 (2013) 6.
[87] Y. Xu, H. Bai, G. Lu, C. Li, G. Shi, Journal of the American Chemical Society, 130 (2008) 5856-5857.
[88] Y. Li, X. Huang, Y. Li, Y. Xu, Y. Wang, E. Zhu, X. Duan, Y. Huang, Scientific reports, 3 (2013).
[89] A.K. Mishra, S. Ramaprabhu, The Journal of Physical Chemistry C, 115 (2011) 14006-14013.
[90] I. Roy, D. Rana, G. Sarkar, A. Bhattacharyya, N.R. Saha, S. Mondal, S. Pattanayak, S. Chattopadhyay, D. Chattopadhyay, RSC Advances, 5 (2015) 25357-25364.
[91] J. Kauppila, P. Kunnas, P. Damlin, A. Viinikanoja, C. Kvarnström, Electrochimica Acta, 89 (2013) 84-89.
[92] J. Molina, A. Zille, J. Fernández, A.P. Souto, J. Bonastre, F. Cases, Synthetic Metals, 204 (2015) 110-121.